

Random Caching Design for Multi-User Multi-Antenna HetNets with Interference Nulling

Tianming Feng, Xuemai Gu, *Member, IEEE*, and Ben Liang, *Fellow, IEEE*

Abstract—The strong interference suffered by users can be a severe problem in cache-enabled networks (CENs) due to the content-centric user association mechanism. To tackle this issue, multi-antenna technology may be employed for interference management. In this paper, we consider a user-centric interference nulling (IN) scheme in two-tier multi-user multi-antenna CEN, with a hybrid most-popular and random caching policy at macro base stations (MBSs) and small base stations (SBSs) to provide file diversity. All the interfering SBSs within the IN range of a user are requested to suppress the interference at this user using zero-forcing beamforming. Using stochastic geometry analysis techniques, we derive a tractable expression for the area spectral efficiency (ASE). A lower bound on the ASE is also obtained, with which we then consider ASE maximization, by optimizing the caching policy and IN coefficient. To solve the resultant mixed integer programming problem, we design an alternating optimization algorithm to minimize the lower bound of the ASE. Our numerical results demonstrate that the proposed caching policy yields performance that is close to the optimum, and it outperforms several existing baselines.

Index Terms—Random caching, HetNets, ZFBF, interference nulling, stochastic geometry.

I. INTRODUCTION

HETEROGENEOUS networks (HetNets) provide an effective framework to meet the exponentially increasing data traffic demand caused by the explosive growth of mobile devices [1], [2]. By densely deploying small base stations (SBSs) along with the existing macro base stations (MBSs), HetNets can boost spatial utilization and thus significantly improve the area spectral efficiency (ASE). However, base station (BS) densification and the consequent spectrum reuse in HetNets can cause heavy burden on backhaul links [3] and strong inter-cell interference [4], which may become bottlenecks on network performance.

To alleviate the backhaul load, an effective solution is to cache popular files at BSs [5]. The paradigm of cache-enabled networks (CENs) is inspired by the fact that a large part of the data traffic is caused by the duplicate downloads of popular files, so that pre-caching the popular files at BSs during off-peak time can significantly reduce the backhaul cost [6]. Moreover, equipping BSs with cache can further improve the network ASE in HetNets [5]. However, because of the limited cache size at BSs, the serving BS of a user may not be geographically its nearest BS, which may lead to strong interference at the user [7]. Therefore, appropriate interference

management techniques are needed to enhance the quality of signals received by users.

Deploying multiple antennas at each BS is a widely-adopted method to address the aforementioned interference problem. With multiple antennas, the link reliability can be ensured by providing spatial diversity or conducting interference nulling (IN) [8]. In addition, the ASE can be further improved by serving multiple users over the same time-frequency resource block (i.e., achieving space division multiple access (SDMA)) [9].

Recently, several works have focused on performance analysis and caching policy design in multi-antenna CENs [10]–[14]. However, [10]–[12] do not consider interference management. In [13], multiple antennas are equipped at each receiver to suppress the received interference in CENs with random caching. However, this receiver-side IN scheme may not be effective when the network is highly densified. In [14], the BSs are grouped into disjoint clusters, and the intra-cluster interference is canceled by BS coordination. However, the number of BSs for interference coordination is fixed, which can be ineffective in practice where different users have different numbers of dominant interferers due to the irregular placement of BSs. Further discussion on related work is given in Section II. Overall, while it is expected that deploying multiple antennas is an effective method for managing interference and improving the ASE of CENs, 1) there has been no formal analysis on the relation between the IN requests received by each BS and the files cached in the network; and 2) it remains an open problem how to jointly design random caching policy and IN to take advantage of the cache resource as well as the antenna resource to improve the network ASE.

In this paper, we consider a two-tier cache-enabled multi-user multi-antenna HetNet, where both MBSs and SBSs are equipped with caches and multiple antennas. We study an IN scheme for the SBS tier, where a part of the spatial degrees-of-freedom (DoF) is used to serve multiple users per channel to improve the network ASE; whereas the remaining DoF is reserved for IN to suppress the dominant interference received by the users. Due to the random caching at SBSs and the adoption of SDMA, the pattern of interference received by each user is complex. Moreover, the IN scheme itself further complicates the interference distribution and the analysis of the ASE. In this context, our main contributions are as follows.

- We analyze the ASE of the aforementioned two-tier cache-enabled multi-user multi-antenna HetNets with a hybrid caching policy and a user-centric IN scheme in the typical interference-limited scenario. Specifically, the most popular caching (MPC) method in the MBS tier and random caching in the SBS tier are used to provide file diversity. All the antennas

T. Feng and X. Gu are with the School of Electronic and Information Engineering, Harbin Institute of Technology, Harbin 150001, China (e-mail: {fengtianming, guxuemai}@hit.edu.cn).

B. Liang is with the Department of Electrical and Computer Engineering, University of Toronto, Toronto, ON M5S 1A1, Canada (e-mail: liang@ece.utoronto.ca).

at MBSs are used to serve multiple users to achieve SDMA, whereas part of the spatial DoF at SBSs is used to implement SDMA, and the remaining DoF is reserved for IN. Due to the high complexity of the ASE expression, we further derive a simple lower bound for it, which is in the form of a sum of linear-fractional functions of the caching probabilities.

- We consider the ASE maximization problem by optimizing the caching policy and the IN coefficient. We separate the problem into two sub-problems, i.e., cache placement optimization and IN coefficient optimization. The first sub-problem is a complicated mixed integer programming problem. By exploiting some of its structural properties, we significantly reduce the computational complexity of the discrete part of this problem. By replacing the ASE with the aforementioned simple lower bound, the continuous part is transformed into a convex problem, which can be effectively solved using KKT conditions. Then, the second sub-problem is effectively solved using line search. Finally, by alternately solving these two sub-problems, we reach a stationary point for maximizing the ASE lower-bound.

- Our simulation results reveal that the proposed solution yields performance that is close to optimal. Specifically, when the signal to interference and noise ratio (SINR) threshold τ is small, caching files according to the uniform distribution will achieve the highest ASE; whereas caching the most popular files is better when τ is large. In general, the proposed caching policy outperforms existing caching strategies.

The rest of this paper is organized as follows. We present a literature survey in Section II. The system model is presented in Section III. Section IV provides a performance analysis of the system, and Section V optimizes the random caching policy and IN coefficient. The numerical results are provided in Section VI, and the conclusions are drawn in Section VII.

Notations: In this paper, vectors and matrices are denoted by bold-face lower-case (e.g., \mathbf{h}) and upper-case (e.g., \mathbf{H}) letters respectively. We use \mathbf{I}_n to denote an $n \times n$ identity matrix. $(\cdot)^T$ and $(\cdot)^H$ denote transpose and Hermitian (or conjugate transpose), respectively. $\mathbf{H}^\dagger = (\mathbf{H}^H \mathbf{H})^{-1} \mathbf{H}^H$ denotes the left pseudo-inverse of \mathbf{H} . \mathbb{R} and \mathbb{C} are used to denote the set of real numbers and complex numbers, respectively. The complex Gaussian distribution with mean μ and covariance σ^2 is denoted by $\mathcal{CN}(0, \sigma^2)$. $\|\mathbf{h}\|$ denotes the Euclidean norm of the vector \mathbf{h} , and $\|\mathbf{H}\|_1$ denotes the L_1 induced norm of the matrix \mathbf{H} , i.e., $\|\mathbf{H}\|_1 = \max_{1 \leq j \leq n} \sum_{i=1}^m |h_{ij}|$ for $\mathbf{H} \in \mathbb{R}^{m \times n}$. $X \stackrel{d}{\sim} Y$ means that X is distributed as Y . $\mathbb{P}[\cdot]$ denotes the probability, while $\mathbb{E}[\cdot]$ is the expectation. $\Gamma(k, \theta)$ denotes the Gamma distribution with shape parameter k and scale parameter θ ; $\Gamma(\cdot)$ denotes the Gamma function; $\mathbb{1}\{\cdot\}$ is the indicator function.

II. RELATED WORKS

A. Caching Policy Design

Caching policy design plays a pivotal role in reaping the benefit of caching. By carefully designing the caching policy, more files can be stored in the network to provide file diversity and thus ensure network performance. In [15]–[17], the authors propose three basic caching policies, i.e.,

MPC, uniform distribution caching (UDC), and independent identical distribution caching (IIDC), respectively. However, these simple caching policies do not take full advantage of the benefit brought by caching. Therefore, the authors of more recent works endeavor to design optimal random caching policies to respectively maximize the hit probability [18]–[20], the successful transmission probability (STP) [10], [21], [22], the traffic offloading gain [14], [23], and the ASE [10], [11], [14]. When adopting a random caching policy, a BS will randomly decide whether to store a file according to its caching probability. It is likely that the serving BS of a user is not geographically its nearest BS. In this case, the interference caused by the nearer BSs will significantly degrade the quality of signal received by the user. Therefore, for CENs with a random caching policy, we need to further consider interference management.

B. Interference Nulling with Multiple Antennas

Multi-antenna communication is a widely-adopted approach to increase SINR. With multiple antennas equipped at each BS, not only the desired signals of users can be boosted, but more effective interference management techniques can be implemented [24]–[27]. Specifically, the authors in [24] propose a cluster-based IN scheme, where all the BSs are grouped into disjoint clusters, and zero-forcing beamforming (ZFBF) is conducted at each BS to mitigate intra-cluster interference. However, the scheme is designed from the perspective of transmitters and does not directly consider each user's needs. To this end, a user-centric IN scheme is proposed for multi-antenna small cell (single-tier) networks in [25], where an IN range is set for each user based on its desired signal strength and interference level. The authors in [26] further extend the IN scheme in [25] to HetNets. The IN schemes considered in [24]–[26] utilize extra spatial DoF at BSs to eliminate interference at users, and data exchange between BSs is avoided. The work in [27] achieves an improvement of SINR from another perspective, i.e., the network MIMO system, where cooperative BSs jointly transmit information to multiple users in the cooperative cluster via coherent beamforming. In this scheme, a BS does not need to reserve extra spatial DoF for IN, but the exchange of user data between cooperative BSs is required. We note that none of [24]–[27] considers caching.

C. Multi-Antenna Cache-Enabled Networks

Random caching policy design in multi-antenna CENs has also been studied in recent literature. In [10], an optimal caching policy is proposed to maximize the STP and ASE in a two-tier CEN, but only MBSs connecting to the core network are equipped with multiple antennas, while the SBSs with caches are equipped with only a single antenna. The authors in [11] consider a multi-tier multi-antenna CEN, where BSs from different tiers have different caching capabilities and are equipped with multiple antennas to serve multiple users via SDMA. A locally optimal caching policy for each tier is obtained by maximizing the potential throughput. The authors in [12] design a locally optimal caching policy in a single-tier multi-antenna CEN considering limited backhaul

capacity. The authors in [13] attempt to perform interference cancellation at the receiver side in CENs. Two types of linear receivers at users are considered, i.e., maximal ratio combining receiver and partial zero-forcing receiver. Only the channel state information (CSI) at receivers is required, so that the burden on the BS can be reduced. In [14], the authors investigate a BS coordination IN scheme for CENs, where a user-centric BS clustering model is proposed to form a BS cluster, and ZFBF is adopted at BSs to null out the interference within the coordination cluster. Optimal caching policies are obtained by maximizing the average fractional offloaded traffic and average ergodic spectral efficiency.

In contrast to these existing works, we focus on the analysis and maximization of the network ASE considering the proposed user-centric IN scheme. Different from [10]–[12], the relation between IN and caching is explored in this work. In contrast to [13], we consider the transmitter-side IN scheme, which is more effective since BSs usually have much more antenna resource than receivers. Moreover, unlike [14], an adjustable IN coefficient is introduced to give the IN scheme more flexibility. Finally, in [13], [14], only one single user is served over each time-frequency resource block (RB), so the spatial DoF provided by multiple antennas is not fully utilized to realize SDMA. In this work, we consider the multi-user scenario, where SDMA is used to further improve the network capacity. All the aforementioned features make our system more complex and more challenging to analyze.

III. SYSTEM MODEL

A. Network and Caching Model

We consider a two-tier cache-enabled multi-antenna HetNet, where a tier of SBSs is overlaid with a tier of MBSs. To avoid inter-tier interference, orthogonal frequencies are adopted at MBSs and SBSs. The locations of MBSs and SBSs are modeled as two independent homogeneous Poisson point processes (PPPs) denoted by Φ_1 and Φ_2 with densities λ_1 and λ_2 , respectively, where $\lambda_1 < \lambda_2$. The users are also distributed in \mathbb{R}^2 according to a PPP Φ_u with density λ_u . Each BS in the k -th tier, $k \in \{1, 2\}$, is equipped with M_k antennas, with transmit power P_k , and can serve U_k users, where $U_k \leq M_k$, simultaneously over one time-frequency RB, i.e., intra-cell SDMA is considered. MBSs are equipped with caches and connected to the core network with limited-capacity backhaul links, whereas SBSs are only equipped with caches. Each user has a single receiving antenna. Full load assumption is considered in this paper, i.e., $\lambda_u \gg \lambda_k, \forall k \in \{1, 2\}$, so that each BS in the k -th tier has at least U_k users connected to it [28]–[30]. When the number of users in each cell from the k -th tier is greater than U_k , the BS will randomly choose U_k users to serve at each time instant. We focus on the performance analysis of a typical user u_0 located at the origin without loss of generality.

We consider a content library containing N different files denoted by $\mathcal{N} = \{1, 2, \dots, N\}$, all files have the same size which equals 1. At any given time instant, for any arbitrary given user, the probability that file n is requested by the user is $a_n \in [0, 1]$, which is called file popularity, satisfying

TABLE I
SUMMARY OF NOTATION

Notation	Description
$\Phi_1, \Phi_2, \Phi_u,$ Φ_u^2	PPPs of MBSs (named as the 1 st tier), SBSs (named as the 2 nd tier), users, and the users served by SBSs.
$\lambda_1, \lambda_2, \lambda_u$	The densities of MBSs, SBSs, and users.
M_k	Number of antennas equipped at BSs in the k -th tier.
P_k	Transmit power of BSs in the k -th tier.
U_k	Number of users served simultaneously by an BS from the k -th tier.
α_k	Path loss exponent for the k -th tier.
$\mathcal{N}, \bar{\mathcal{N}}, \mathcal{N}_1,$ N_1, \mathcal{N}_2, N_2	Set of all files, size of \mathcal{N} , the first sub-set of files, size of \mathcal{N}_1 , the second sub-set of files, size of \mathcal{N}_2 .
$\mathcal{N}_c, N_c,$ \mathcal{N}_b, N_b	Set of files stored in the SBS tier, size of \mathcal{N}_c , set of files not stored in the network, size of \mathcal{N}_b .
C_k, C_b	Cache size of each BS in the k -th tier, backhaul capacity of each MBS.
a_n	The popularity of file n .
T_n, \mathbf{T}	Caching probability for file n , caching probability vector.
$\mathcal{I}, I, \mathcal{I}_i,$ \mathcal{I}^n, I^n	Set of file combinations, size of \mathcal{I} , the i -th combination in \mathcal{I} , set of combinations containing file n , size of \mathcal{I}^n .
p_i	Probability of an SBS storing \mathcal{I}_i .
x_{10}, x_{20}	Serving BSs of an MBS-user and SBS-user, respectively.
Z_1, Z_2	The distance between an MBS-user or SBS-user and its serving BS.
L_b	Backhaul load of an MBS.
μ	The IN coefficient.
$\Theta_x, \bar{\Theta}$	Number of IN requests received by an SBS x , mean number of IN received by an SBS.
$\Phi_2^a, \Phi_2^b, \Phi_2^c,$ $\lambda_2^a, \lambda_2^b, \lambda_2^c,$ $\Omega_a, \Omega_b, \Omega_c$	Sets of interfering SBSs of Type-A, Type-B, and Type-C; densities of $\Phi_2^a, \Phi_2^b, \Phi_2^c$; corresponding distance intervals of $\Phi_2^a, \Phi_2^b, \Phi_2^c$.
$\Upsilon_{n,k}$	Received SINR of a user requesting file n and served by the k -th tier.
g_{0k}, g_{xk}	Desired channel gain in the k -th tier, interfering channel gain in the k -th tier.
τ	SINR threshold.
ε	IN missing probability.

$\sum_{n \in \mathcal{N}} a_n = 1$. For example, it has been observed that the popularity of file n follows a Zipf distribution [10], [11], [13], i.e., $a_n = \frac{n^{-\gamma_z}}{\sum_{n \in \mathcal{N}} n^{-\gamma_z}}$, $n \in \mathcal{N}$, where γ_z is the Zipf exponent. The analysis in this work is applicable to any popularity distribution. Without loss of generality, we assume that a file of smaller index has higher popularity, i.e., $a_1 > a_2 > \dots > a_N$. Denote by $C_k, k \in \{1, 2\}$ the cache size of each BS in the k -th tier, and C_b the backhaul link capacity of each MBS.

For the hybrid caching policy, we observe the following principles: 1) a high cache hit probability can be ensured by storing the most popular files at all MBSs, since MBSs are usually equipped with large cache space, the frequently requested files can always be served by the nearest MBS of a user; 2) spatial file diversity can be fully exploited by storing the less popular files at SBSs randomly, since the density of the SBS is comparatively high so that more files can be stored at the SBS tier; and 3) the requests for the files not stored at any BS can be satisfied via the backhaul links of MBSs.

Therefore, we divide the content library into two disjoint portions: the first sub-set of files contains the N_1 most popular files, which is denoted by $\mathcal{N}_1 \triangleq \{1, 2, \dots, N_1\}$; the second sub-set $\mathcal{N}_2 \triangleq \{N_1+1, N_1+2, \dots, N\}$ contains the remaining $N_2 \triangleq |\mathcal{N}_2|$ files. For MBSs, the most popular caching policy

is employed, where all the N_1 files from \mathcal{N}_1 are stored at every MBS; thus we explicitly require that $C_1 = N_1$. For SBSs, we adopt a random caching policy, where each SBS randomly chooses C_2 different files from \mathcal{N}_2 to store. Denote by $T_n \in [0, 1]$ the probability that an SBS caches the file n . We further define $\mathcal{N}_c \triangleq \{n \in \mathcal{N}_2 : T_n > 0\}$, which is the set of files that can be stored in the SBS tier, with $N_c \triangleq |\mathcal{N}_c|$. Then, $\mathbf{T} \triangleq [T_n]_{n \in \mathcal{N}_c}$ denotes the caching probability vector for the SBS tier, which is identical for all the SBSs. Let $\mathcal{N}_b \triangleq \mathcal{N}_2 \setminus \mathcal{N}_c$ be the set of files not cached at any BS in the network, with $N_b \triangleq |\mathcal{N}_b|$. The backhaul link of each MBS is used to retrieve the files that are requested by its associated users but not stored at its local caches from the core network. Thus, the set of files needed to be retrieved from the core network of an MBS is a subset of \mathcal{N}_b .

With the random caching policy, each SBS stores C_2 different files out of \mathcal{N}_c . Thus, there are totally $I \triangleq \binom{N_c}{C_2}$ different combinations that can be chosen. Denote by $\mathcal{I} \triangleq \{1, 2, \dots, I\}$ this set of I combinations. Let \mathcal{I}_i be the i -th combination from \mathcal{I} . Let $\zeta_{i,n} = 1$ indicate that the file n is included in combination i , and $\zeta_{i,n} = 0$ otherwise; thus $\sum_{n \in \mathcal{N}_c} \zeta_{i,n} = C_2$. Let $\mathcal{I}^n \triangleq \{i \in \mathcal{I} : \zeta_{i,n} = 1\}$ be the set of $I^n \triangleq \binom{N_c-1}{C_2-1}$ combinations containing file n . Let p_i be the probability that an SBS chooses \mathcal{I}_i to store; then we have

$$T_n = \sum_{i \in \mathcal{I}^n} p_i, \quad n \in \mathcal{N}_c. \quad (1)$$

B. User Association

Based on the aforementioned hybrid caching policy, a user connects to a BS depending on the file it requests. Specifically, a user requesting file $n \in \mathcal{N}_1$ will connect to its nearest MBS; if the requested file n of a user is stored at the SBS tier, i.e., $n \in \mathcal{N}_c$, the user will connect to its nearest SBS storing a combination $i \in \mathcal{I}^n$ (containing file n), and is referred to as an SBS-user; otherwise, a user will be served by its nearest MBS via the backhaul link. A user served by an MBS is referred to as an MBS-user. Denote by x_{10} (resp. x_{20}) the location of the serving BS of a user if it is an MBS-user (resp. SBS-user).

In a multiuser MIMO system, when determining its potential connecting users, a BS normally uses its total transmit power to broadcast reference signals via a single antenna, and the multiuser beamforming is only conducted after user association [28], [29]. A user will choose a BS that can offer the maximum long-term average receive power for its requested file to connect. Note that for an MBS-user, the serving BS is its geographically nearest MBS. However, for an SBS-user, the serving BS may not be its nearest SBS, due to the random caching policy. This user association mechanism is referred to as *content-centric association*, which is different from the distance-based association adopted in traditional networks [30], [31]. Therefore, the interference caused by the SBSs that are closer to the user than the serving SBS needs to be carefully handled. To this end, in this paper, we consider a *user-centric interference nulling scheme*, which will be elaborated on later.

Denote by L_b the *backhaul load* of an MBS, which is the number of different files requested by the users served by the

backhaul link of the MBS. Due to the limited backhaul link capacity, each MBS can only retrieve at most C_b different uncached files requested by its associated users from the core network. If $L_b \leq C_b$, all the requested uncached files can be retrieved via the backhaul link; otherwise the MBS will uniformly randomly select C_b different files to retrieve. The selected uncached files will firstly be retrieved from the core network by the MBS via its backhaul link, and then be passed on to the requesting users.

C. Interference Nulling Scheme

We will now elaborate on the user-centric interference nulling scheme used to suppress the interference from non-serving SBSs in the SBS tier. If the typical user u_0 requesting file n is an SBS-user, the interference it receives mainly comes from 1) the SBSs that do not store file n , and are closer to u_0 than its serving SBS; 2) all SBSs that are further to u_0 than its serving SBS. To suppress the interference, the user will send an IN request to all the interfering SBSs within distance μZ_2 , which is called the *IN range*, where $\mu \in [0, +\infty)$ is referred to as the *IN coefficient*, and Z_2 is the distance between u_0 and its serving SBS.

As shown in Fig. 1, all the SBSs (except the serving SBS) in the red dash line circle will receive an IN request from the typical user. When an SBS receives IN requests, it will use its available antennas to suppress its interference at the requesting users. However, due to the limited spatial DoF, each SBS can only satisfy at most $M_2 - U_2$ IN requests. Let Θ_x be the number of IN requests received by an SBS located at x . If $\Theta_x \leq M_2 - U_2$, all the IN requests received can be satisfied; otherwise the SBS will uniformly randomly choose $M_2 - U_2$ users to suppress the interference.

With this IN scheme, when $0 \leq \mu < 1$ (resp. $\mu \geq 1$), all the interfering SBSs of the typical user can be divided into three parts: the interfering SBSs within the circle of radius μZ_2 (resp. Z_2); the interfering SBSs within the annulus from radius μZ_2 (resp. Z_2) to Z_2 (resp. μZ_2); and the remaining interfering SBSs outside the circle of radius Z_2 (resp. μZ_2), which correspond to Type-A, Type-B, and Type-C shown in Fig. 1, respectively. Let Φ_2^a , Φ_2^b , and Φ_2^c denote the set of interfering SBSs of Type-A, Type-B, and Type-C, respectively. We have $\Phi_2^i \triangleq \{x | x \in \Phi_2 \setminus \{x_{20}\}, \|x\| \in \Omega_i\}$, $i \in \{a, b, c\}$, where $\Omega_a = [0, \min\{Z_2, \mu Z_2\})$, $\Omega_b = [\min\{Z_2, \mu Z_2\}, \max\{Z_2, \mu Z_2\})$, and $\Omega_c = [\max\{Z_2, \mu Z_2\}, +\infty)$ are three distance intervals.

From the system model illustrated above, we can observe that the choice of \mathcal{N}_c , the design of \mathbf{T} , and the value of μ will jointly affect the performance of the network. Therefore, we will set $(\mathcal{N}_c, \mathbf{T}, \mu)$ to be the design parameters.

D. Signal Model

In this paper, we adopt ZFBF to serve multiple users over one time-frequency RB as well as to satisfy the IN requests for SBS-users. Perfect CSI at the transmitter is assumed. For each BS, equal power is allocated to its associated users. For

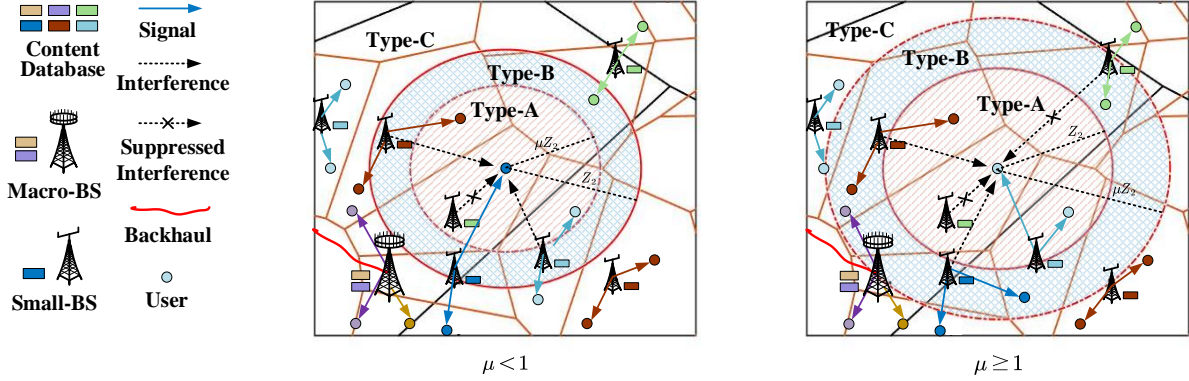


Fig. 1. Network model. The two network tiers correspond to two Voronoi tessellations with black and brown solid lines, respectively. The typical user is located at the origin, the color of whom represents the file it requests. Three types of interfering SBSs are shown in the figure, and the interfering SBSs in the red dash circle will receive an IN request from the typical user.

the typical user u_0 located at the origin and served by BS at x , the received signal is

$$y_{0x} = \sqrt{\frac{P_{\nu(x)}}{U_{\nu(x)}}} Z_{\nu(x)}^{-\frac{\alpha_{\nu(x)}}{2}} \mathbf{h}_{0x}^H \mathbf{F} \mathbf{s}_x + \sum_{x_m \in \tilde{\Phi}_{\nu(x)}} \sqrt{\frac{P_{\nu(x)}}{U_{\nu(x)}}} \|x_m\|^{-\frac{\alpha_{\nu(x)}}{2}} \mathbf{h}_{0x_m}^H \mathbf{F} x_m + n_0, \quad (2)$$

where $\nu(x)$ returns the index of tier to which a BS located at x belongs, i.e., $\nu(x) = k$ iff $x \in \Phi_k$; Z_1 (or Z_2) denotes the distance between u_0 and its serving MBS (or SBS); $\alpha_k > 2$ denotes the path-loss exponent; $\tilde{\Phi}_{\nu(x)}$ is the set of interfering BSs defined by $\tilde{\Phi}_1 = \Phi_1 \setminus \{x\}$ if $\nu(x) = 1$, and $\tilde{\Phi}_2 = \Phi_2^a \cup \Phi_2^b \cup \Phi_2^c$ if $\nu(x) = 2$; \mathbf{h}_{ix} is the channel coefficient vector from the BS located at x to the user i , and satisfies $\mathbf{h}_{ix} \in \mathcal{CN}(\mathbf{0}_{M_{\nu(x)} \times 1}, \mathbf{I}_{M_{\nu(x)}})$; $\mathbf{s}_x = [s_{1x}, s_{2x}, \dots, s_{U_{\nu(x)}x}]^T \in \mathbb{C}^{U_{\nu(x)} \times 1}$ is the complex symbol vector sent by the BS located at x to its $U_{\nu(x)}$ users; $\mathbf{F} = [\mathbf{f}_{1x}, \mathbf{f}_{2x}, \dots, \mathbf{f}_{U_{\nu(x)}x}] \in \mathbb{C}^{M_{\nu(x)} \times U_{\nu(x)}}$ is the precoding matrix of BS x for its $U_{\nu(x)}$ served users, $n_0 \stackrel{d}{\sim} \mathcal{CN}(0, \sigma^2)$ is the additive white Gaussian noise.

By utilizing ZFBF, each MBS can simultaneously serve U_1 users over one time-frequency RB; while the SBS located at x can simultaneously serve U_2 users as well as suppress the interference at other $\min\{\Theta_x, M_2 - U_2\}$ users. The precoding vector is given by

$$\mathbf{f}_{ix} = \frac{(\mathbf{I}_{M_{\nu(x)}} - \mathbf{H}_{-ix} \mathbf{H}_{-ix}^\dagger) \mathbf{h}_{ix}}{\|(\mathbf{I}_{M_{\nu(x)}} - \mathbf{H}_{-ix} \mathbf{H}_{-ix}^\dagger) \mathbf{h}_{ix}\|_2}, \quad (3)$$

where $\mathbf{H}_{-ix} = [\mathbf{h}_{1x}, \dots, \mathbf{h}_{(i-1)x}, \mathbf{h}_{(i+1)x}, \dots, \mathbf{h}_{\Lambda x}]$, with $\Lambda = U_{\nu(x)} + \min\{\Theta_x, M_{\nu(x)} - U_{\nu(x)}\}$. If the serving BS of a user located at x is an MBS, $\Theta_x = 0$, since there is no IN request sent to the MBS.

Suppose u_0 requests file n at the current time instant. Then, the received SINR at u_0 is

$$\Upsilon_{n,\nu(x)} = \frac{\frac{P_{\nu(x)}}{U_{\nu(x)}} g_{0\nu(x)} Z_{\nu(x)}^{-\alpha_{\nu(x)}}}{\sum_{x_m \in \tilde{\Phi}_{\nu(x)}} \frac{P_{\nu(x)}}{U_{\nu(x)}} g_{x_m\nu(x)} \|x_m\|^{-\alpha_{\nu(x)}} + \sigma^2}, \quad (4)$$

where x represents x_{10} (resp. x_{20}) if u_0 is an MBS-user (resp. SBS-user); $g_{0k} \triangleq |\mathbf{h}_{0x_{k0}}^H \mathbf{f}_{0x_{k0}}|^2$, $k \in \{1, 2\}$, is the effective channel gain of the desired signal from x_{k0} , which follows $g_{0k} \stackrel{d}{\sim} \Gamma(D_k, 1)$ [30], with $D_k = \max\{M_k - U_k + 1 - \Theta_{x_{k0}}, 1\}$, and $\Theta_{x_{10}} = 0$; $g_{x_k} \triangleq |\mathbf{h}_{0x_m}^H \mathbf{F} x_m|^2$ is the interfering channel gain between u_0 and the BS x_m from the k -th tier, which follows $g_{x_k} \stackrel{d}{\sim} \Gamma(U_k, 1)$ [30].

E. Performance Metric

We use the ASE as a metric to measure the network capacity. The ASE describes the average achieved data rate per unit area normalized by the transmission bandwidth, with a unit bit/s/Hz/m², which is defined as [28]

$$\text{ASE}(\mathcal{N}_c, \mathbf{T}, \mu) = \log_2(1 + \tau) \left(\lambda_1 U_1 q_1(\mathcal{N}_c) + \lambda_2 U_2 q_2(\mathcal{N}_c, \mathbf{T}, \mu) \right), \quad (5)$$

where τ is some predefined SINR threshold, and

$$q_1(\mathcal{N}_c) \triangleq \left(\sum_{n \in \mathcal{N}_1} a_n + \sum_{n \in \mathcal{N}_b} a_n \xi(N_b) \right) \mathbb{P}[\Upsilon_{n,1} \geq \tau], \quad (6)$$

$$q_2(\mathcal{N}_c, \mathbf{T}, \mu) \triangleq \sum_{n \in \mathcal{N}_c} a_n \mathbb{P}[\Upsilon_{n,2} \geq \tau], \quad (7)$$

represent the STP of u_0 as an MBS-user or an SBS-user, respectively, where $\xi(x)$ is the probability that a requested file is successfully retrieved over the backhaul link given the

¹When $k = 1$, each MBS serves $U_1 = M_1$ users over the same time-frequency RB. Therefore, $D_1 = 1$, $g_{01} \stackrel{d}{\sim} \Gamma(1, 1)$, which is the exponential distribution with unit mean.

backhaul load is x . Since we consider a full-loaded network, the backhaul load of each MBS should always be full, i.e., $L_b \equiv N_b$, we have $\xi(x) = \min\{1, \frac{C_b}{x}\}$. Here, the STP is an intermediate metric, which represents the probability that the received SINR at the typical user exceeds a given threshold τ .

A summary of the frequently mentioned symbols is provided in Table I.

IV. DERIVATION OF ASE($\mathcal{N}_c, \mathbf{T}, \mu$)

In this section, we will derive the expression for ASE under the proposed IN scheme for some given ($\mathcal{N}_c, \mathbf{T}, \mu$), and use Monte Carlo simulation to verify the analytical results. From (5), we see that to compute ASE($\mathcal{N}_c, \mathbf{T}, \mu$), it suffices to derive the expressions for the STPs $q_1(\mathcal{N}_c)$ and $q_2(\mathcal{N}_c, \mathbf{T}, \mu)$. Furthermore, in modern dense wireless networks, the strength of interference is much greater than that of background thermal noise. Therefore, it is reasonable to neglect the noise. In the sequel, we focus on the performance analysis of the interference-limited scenario, i.e., $\sigma^2 = 0$ in (4).

A. Derivation of MBS STP $q_1(\mathcal{N}_c)$

When the typical user is an MBS-user, the serving BS is its nearest MBS. Since the frequency bands used by MBS and SBS are orthogonal, there is no inter-tier interference, and all the interference comes from the MBSs that are farther away from the typical user than the serving MBS. By deriving the probability distribution function (PDF) of $\Upsilon_{n,1}$ in (4), we can obtain the STP for the MBS tier.

As shown in Appendix A, the STP for the MBS tier is given by

$$q_1(\mathcal{N}_c) = \left(\sum_{n \in \mathcal{N}_1} a_n + \sum_{n \in \mathcal{N}_b} a_n \xi(N_b) \right) \Psi_1, \quad (8)$$

with

$$\Psi_1 = \frac{1}{1 + F_1(\tau)}, \quad (9)$$

where $\xi(N_b) = \min\{1, \frac{C_b}{N_b}\}$ and $F_j(x)$ is defined in (10) with ${}_2F_1(a, b; c; d)$ denoting the Gauss hypergeometric function:

$$F_j(x) = {}_2F_1\left(-\frac{2}{\alpha_j}, U_j; 1 - \frac{2}{\alpha_j}; -x\right) - 1, \quad j \in \{1, 2\}. \quad (10)$$

From (8), we can observe that the impact of the caching policy on the STP for the MBS tier is mainly reflected by the backhaul load, which is only determined by the choice of \mathcal{N}_b (or equivalently \mathcal{N}_c).

B. Number of IN Requests Received by an SBS

Before deriving the SBS STP $q_2(\mathcal{N}_c, \mathbf{T}, \mu)$, we first need to calculate the probability mass function (PMF) of the number of IN requests received by the serving SBS of a user. The content-centric association mechanism adopted in this work allows the IN coefficient μ to be smaller than 1, and the interfering SBSs are further categorized into Type-A, Type-B, and Type-C, making the network much more complicated and more challenging to analyze than that in [25].

To allow feasible performance analysis of the network, we assume that 1) the users served by the SBS tier form a homogeneous PPP Φ_u^2 , and is a thinning of Φ_u ; 2) Φ_u^2 is independent from all the SBSs Φ_2 ; and 3) the numbers of IN requests received by different SBSs are independent. Note that the first and second assumptions have been considered in previous works [25], [26], [32]. The third assumption is also adopted in [25], [26], where the accuracy of these three assumptions is verified. With these assumptions, the distribution of served users and that of SBSs are decoupled so that the system model becomes tractable. Our numerical results will further demonstrate that these assumptions allow accurate analysis in our system.

With the above assumptions, it is clear that the number of IN requests received by an SBS, denoted by Θ , is a Poisson random variable with PMF

$$p_\Theta(\theta, N_c, \mu) = \frac{(\bar{\Theta})^\theta}{\theta!} e^{-\bar{\Theta}}, \quad (11)$$

where $\bar{\Theta}$ is the mean of the number of IN requests received by an SBS. We further observe that $\bar{\Theta}$ is approximately given by

$$\bar{\Theta} = \frac{N_c U_2 \mu^2}{C_2} - \min\{\mu^2, 1\} U_2. \quad (12)$$

The detailed derivation can be found in Appendix B.

From (11) and (12), we can find that the average number of requests received by an SBS is only related to the number of files cached at the SBS tier N_c , the cache size at each SBS C_2 , the spatial DoF allocated for SDMA by each SBS U_2 , and the IN coefficient μ . Specifically, when N_c increases, more files can be cached at SBSs, but, due to the limitation of cache size C_2 , the probability of each file being cached will decrease, leading to a larger distance between the user and its serving SBS. Therefore, more IN requests will be received at SBSs, i.e., $\bar{\Theta}$ increases. Similarly, increasing the cache size C_2 will increase the probability of files being cached, and hence, shorten the distance between users and files, so that $\bar{\Theta}$ decreases. Increasing U_2 will make more users connected to the network, resulting in a higher $\bar{\Theta}$. Moreover, a larger μ will make users send IN requests to more SBSs, contributing to a larger number of requests received at each SBS. In the sequel, with a slight abuse of notation, we use $p_\Theta(\theta)$ to denote $p_\Theta(\theta, N_c, \mu)$.

The PMF in (11) is verified by simulation shown in Fig. 2. In Fig. 2, we define $\rho \triangleq \frac{\lambda_u}{\lambda_2 U_2}$ to characterize the user load of each SBS. From Fig. 2, we can observe that the analytical expression given in (11) matches well with simulation especially when the load is high, and it is more accurate with smaller μ and N_c .

C. Derivation of SBS STP $q_2(\mathcal{N}_c, \mathbf{T}, \mu)$

To obtain an expression for $q_2(\mathcal{N}_c, \mathbf{T}, \mu)$, we start from calculating the probability that an SBS has received an IN request from u_0 but is unable to satisfy it, which is denoted by ε and referred to as the *IN missing probability*. We consider an interfering SBS B_0 located in the IN range of u_0 . Then it has received the request from u_0 . Let's suppose it receives $\Theta_0 =$

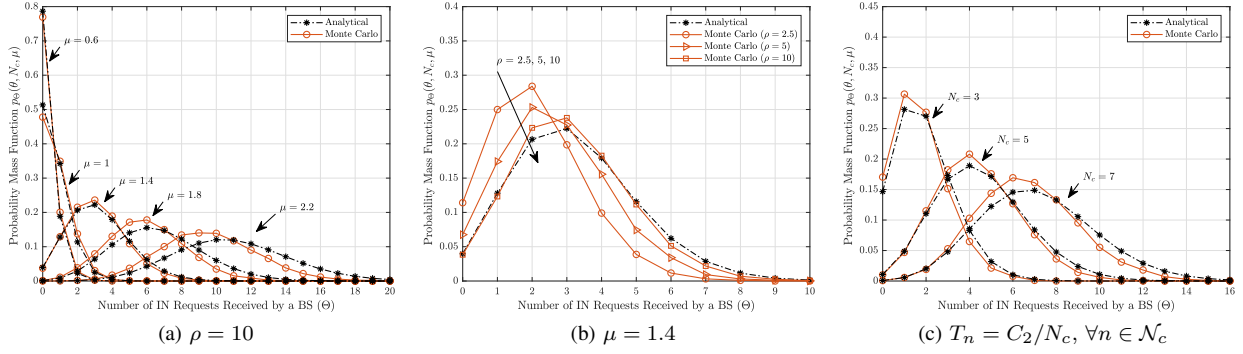


Fig. 2. The probability mass function of Θ , i.e., $p_{\Theta}(\theta, N_c, \mu)$. The default setting of the parameters is $M_1 = 8, M_2 = 6, U_1 = 8, U_2 = 2, P = [46, 23]$ dBm, $\alpha_1 = \alpha_2 = 4, \lambda_1 = 1 \times 10^{-4} \text{ m}^{-2}, \lambda_2 = 5 \times 10^{-4} \text{ m}^{-2}, \lambda_u = 0.01 \text{ m}^{-2}$ (i.e., $\rho = 10$), $N = 12, C_1 = 4, C_2 = 3, C_b = 2, \mathcal{N}_1 = \{1, 2, 3, 4\}, \mathcal{N}_c = \{5, 6, 7, 8\}, \mathcal{N}_b = \{9, 10, 11, 12\}, \mathbf{T} = [0.9, 0.8, 0.7, 0.6], \gamma_z = 0.8, \mu = 1.4$. For the sub-figure (c), uniform caching is adopted and the most popular N_c files in \mathcal{N}_2 are cached with probability $T_n = C_2/N_c$. The Monte Carlo results are obtained by averaging 5×10^4 independent random realizations with map size $2 \times 2 \text{ km}^2$.

θ_0 more IN requests from other users, if $\theta_0 + 1 > M_2 - U_2$, the SBS will randomly choose $M_2 - U_2$ requests to satisfy, and hence, the request from u_0 will be denied with probability $\frac{\theta_0 + 1 - (M_2 - U_2)}{\theta_0 + 1}$. We note that all the served SBS-users form a PPP and whether or not a served SBS-user sends IN request to its interfering SBSs is independent of others. Thus, given that B_0 has received the request from u_0 , Θ_0 follows the same PMF as (11), due to Slivnyak's theorem [33]. Therefore, ε is given by

$$\varepsilon = \sum_{\theta_0=M_2-U_2}^{\infty} \frac{\theta_0 + 1 - (M_2 - U_2)}{\theta_0 + 1} p_{\Theta}(\theta_0). \quad (13)$$

Then, as shown in Appendix C, the STP for the SBS tier is

$$q_2(\mathcal{N}_c, \mathbf{T}, \mu) = \sum_{n \in \mathcal{N}_c} a_n \Psi_2(T_n, N_c, \mu), \quad (14)$$

where $\Psi_2(T_n, N_c, \mu)$ is given by

$$\begin{aligned} & \Psi_2(T_n, N_c, \mu) \\ &= T_n \sum_{\theta=0}^{M_2-U_2-1} p_{\Theta}(\theta) \|\mathbf{W}_{D_2}(T_n, N_c, \mu)^{-1}\|_1 + \frac{p_{\Theta}^s T_n}{T_n + w_0}, \end{aligned} \quad (15)$$

with $D_2 = M_2 - U_2 + 1 - \theta$; $p_{\Theta}(\theta)$ is given by (11); $p_{\Theta}^s \triangleq \frac{\gamma(M_2 - U_2, \bar{\Theta})}{\Gamma(M_2 - U_2)}$ with $\bar{\Theta}$ given by (12); $\gamma(s, x) = \int_0^x t^{s-1} e^{-t} dt$ is the lower incomplete Gamma function; $\mathbf{W}_{D_2}(T_n, N_c, \mu)$ is a $D_2 \times D_2$ lower Toeplitz matrix, given by

$$\mathbf{W}_{D_2}(T_n, N_c, \mu) = \begin{bmatrix} T_n + w_0 & & & \\ -w_1 & T_n + w_0 & & \\ \vdots & \vdots & \ddots & \\ -w_{D_2-1} & -w_{D_2-2} & \cdots & T_n + w_0 \end{bmatrix}, \quad (16)$$

the elements of which, i.e., w_0 and w_m for $m \geq 1$, are given by

$$w_0 = \varepsilon(1 - T_n)G(\tau) + a(1 - \varepsilon)\mu^2 F_2\left(\frac{\tau}{\mu^{\alpha_2}}\right) + bT_n F_2(\tau), \quad (17)$$

$$w_m = \frac{2(U_2)_m}{m!} \left\{ \varepsilon(1 - T_n) \frac{1}{\alpha_2} \tau^{\frac{2}{\alpha_2}} B\left(m - \frac{2}{\alpha_2}, U_2 + \frac{2}{\alpha_2}\right) \right.$$

$$\left. + a(1 - \varepsilon)\mu^2 \tilde{F}_m\left(\frac{\tau}{\mu^{\alpha_2}}\right) + bT_n \tilde{F}_m(\tau) \right\}, \quad (18)$$

with $F_j(x)$ given in (10); a and b are given by

$$a = \begin{cases} 1 - T_n & \mu < 1, \\ 1 & \mu \geq 1, \end{cases} \quad b = \begin{cases} 1 & \mu < 1, \\ \varepsilon & \mu \geq 1; \end{cases} \quad (19)$$

$G(x)$ is given by

$$G(x) = \frac{\Gamma\left(1 - \frac{2}{\alpha_2}\right) \Gamma\left(U_2 + \frac{2}{\alpha_2}\right)}{\Gamma(U_2)} x^{\frac{2}{\alpha_2}}; \quad (20)$$

$(U)_m = U(U+1) \cdots (U+m-1)$ is the Pochhammer symbol; $B(x, y)$ is the Beta function; and $\tilde{F}_k(x)$ is

$$\tilde{F}_k(x) = \frac{x^k}{\alpha_2 k - 2} {}_2F_1\left(U_2 + k, k - \frac{2}{\alpha_2}; k - \frac{2}{\alpha_2} + 1; -x\right). \quad (21)$$

From the expression for $q_2(\mathcal{N}_c, \mathbf{T}, \mu)$, we can observe that the STP of the SBS tier is affected by the design parameters $(\mathcal{N}_c, \mathbf{T}, \mu)$ in an extremely complicated manner. Specifically, the number of elements in \mathcal{N}_c , i.e., N_c , and the IN coefficient μ will affect Θ , so that the PMF $p_{\Theta}(\theta)$ and the IN missing probability ε are affected. Serving as the weights of summation in (15), $p_{\Theta}(\theta)$ will exert an influence on $\Psi_2(T_n, N_c, \mu)$ directly. Whereas ε will affect the Toeplitz matrix $\mathbf{W}_{D_2}(T_n, N_c, \mu)$ firstly, and then puts an impact on $\Psi_2(T_n, N_c, \mu)$. In terms of T_n , however, it only affects $\mathbf{W}_{D_2}(T_n, N_c, \mu)$ directly and has no influence on Θ . Note that the result given in (14) is a generalized version of that in [25] with further considering the random caching policy and SDMA at the SBSs. By plugging $T_n = 1$ for $\forall n \in \mathcal{N}_c$, and $U_2 = 1$ into (14), the expression for $q_2(\mathcal{N}_c, \mathbf{T}, \mu)$ degrades into the STP obtained in [25].

We note that, by combining (8), (14), and (5), we can obtain the final expression for $\text{ASE}(\mathcal{N}_c, \mathbf{T}, \mu)$.

D. Special Case Where $U_2 = M_2$

In this subsection, we consider a special case where all the available DoF of each SBS is used for SDMA, so that there is no antenna allocated for IN, i.e., $U_2 = M_2$. In this case, we can

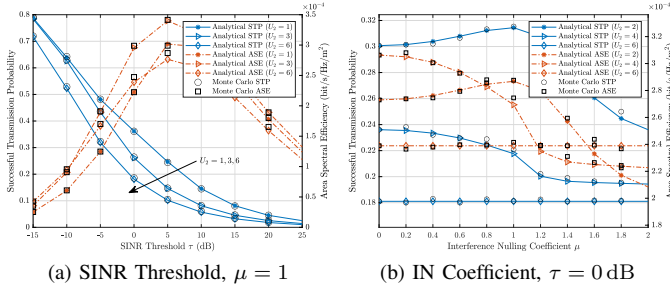


Fig. 3. The STP and ASE versus SINR threshold τ and IN coefficient μ . The simulation parameters are set to be the same as in Fig. 2.

obtain a much simplified closed-form expression for the ASE. In particular, the conditional STP $\Psi_2(T_n, N_c, \mu)$ degrades into

$$\Psi_2^{sp}(T_n) = \frac{T_n}{(1 - G(\tau) + F_2(\tau))T_n + G(\tau)}. \quad (22)$$

By replacing $\Psi_2(T_n, N_c, \mu)$ with $\Psi_2^{sp}(T_n)$ in (14), and considering (5) and (8), $ASE^{sp}(\mathcal{N}_c, \mathbf{T})$ can be obtained.

Note that (22) has a similar formation to Lemma 4 in [7], where a single-input single-output network (with $M_k = U_k = 1$ for all $k \in \{1, 2\}$) is considered. From (22), we can observe that given \mathcal{N}_c , the design parameter T_n is separated from other network parameters such as α_2 , U_2 , and τ . Besides, $ASE^{sp}(\mathcal{N}_c, \mathbf{T})$ is a concave function with respect to (w.r.t.) T_n , for $\forall n \in \mathcal{N}_c$. Therefore, given \mathcal{N}_c , when optimizing \mathbf{T} to maximize the metric $ASE^{sp}(\mathcal{N}_c, \mathbf{T})$, the complexity of the solution can be significantly reduced by using KKT conditions. Unfortunately, optimizing the ASE for the general case of $U_2 < M_2$ is much harder, as will be shown in Section V.

E. Numerical Validation

For numerical validation, Fig. 3 plots the total STP and ASE versus the SINR threshold τ , the IN coefficient μ , and the number of users U_2 served simultaneously by an SBS. Here, the total STP is defined as $q(\mathcal{N}_c, \mathbf{T}, \mu) = q_1(\mathcal{N}_c) + q_2(\mathcal{N}_c, \mathbf{T}, \mu)$. We compare the above ASE analysis with Monte Carlo simulation results. Fig. 3 shows that the analytical expressions for $q(\mathcal{N}_c, \mathbf{T}, \mu)$ and $ASE(\mathcal{N}_c, \mathbf{T}, \mu)$ match the simulation results, even though some approximations have been used (cf. Section IV). Therefore, in the sequel, we will focus on the analysis and optimization for the analytical expressions obtained in this section. Fig. 3(b) shows that for the special case where $U_2 = M_2$, the STP and ASE are independent of μ ; otherwise, the variation tendency of the STP with μ is similar to that of the ASE with μ , and μ should be carefully designed to achieve optimal network performance.

V. AREA SPECTRAL EFFICIENCY MAXIMIZATION

In this section, we will maximize the ASE by jointly optimizing the parameters $(\mathcal{N}_c, \mathbf{T}, \mu)$. Specifically, the optimization problem can be formulated as follows.

Problem 1 (ASE Optimization Problem):

$$ASE^* = \max_{\mathcal{N}_c, \mathbf{T}, \mu} ASE(\mathcal{N}_c, \mathbf{T}, \mu)$$

$$\text{s.t. } N_c \geq C_2, \quad (23a)$$

$$0 \leq T_n \leq 1, \quad \sum_{n \in \mathcal{N}_c} T_n = C_2, \quad (23b)$$

$$\mu \geq 0. \quad (23c)$$

In the sequel, we use \mathcal{N}_c^* , \mathbf{T}^* , and μ^* to denote the optimal value of variables \mathcal{N}_c , \mathbf{T} , and μ , respectively. By optimizing the cache placement parameters \mathcal{N}_c and \mathbf{T} as well as the IN coefficient μ , the objective function in Problem 1 can be maximized. However, the feasible sets for \mathbf{T} and μ are continuous whereas that for \mathcal{N}_c is discrete, making Problem 1 a mixed integer programming problem. To effectively solve Problem 1, we next partition it into two sub-problems, i.e., *cache placement optimization problem* and *IN coefficient optimization problem*, which will be solved alternately.

A. Cache Placement Optimization

First, we consider the cache placement optimization problem with a given μ , which can be formulated as follows.

Problem 2 (Cache Placement Optimization):

$$ASE^*(\mu) = \max_{\mathcal{N}_c, \mathbf{T}} ASE(\mathcal{N}_c, \mathbf{T}, \mu) \quad (24)$$

$$\text{s.t. } (23a), (23b).$$

Note that Problem 2 is still a mixed integer programming problem where the discrete part is to choose the elements of the set \mathcal{N}_c , and the continuous part is to design the caching probability vector \mathbf{T} .

We will decompose the ASE into the MBS-tier and SBS-tier components as $ASE_1 = \lambda_1 U_1 q_1(\mathcal{N}_c) \log_2(1 + \tau)$ and $ASE_2 = \lambda_2 U_2 q_2(\mathcal{N}_c, \mathbf{T}, \mu) \log_2(1 + \tau)$. Then, Problem 2 has the following equivalent form:

Problem 3 (Equivalent Problem):

$$ASE^*(\mu) = \max_{\mathcal{N}_c} ASE_1(\mathcal{N}_c) + ASE_2^*(\mathcal{N}_c, \mu) \quad (25)$$

$$\text{s.t. } (23a),$$

$$ASE_2^*(\mathcal{N}_c, \mu) = \max_{\mathbf{T}} ASE_2(\mathcal{N}_c, \mathbf{T}, \mu) \quad (26)$$

$$\text{s.t. } (23b).$$

For the discrete optimization problem in (25), there are totally $\sum_{N_c=C_2}^{N_2} \binom{N_2}{N_c} = O(N_2^{N_2})$ different choices in the feasible set. Even if $ASE_2^*(\mathcal{N}_c, \mu)$ is given for each choice of \mathcal{N}_c , the computation complexity can be prohibitive when N_2 and N_c are large. On the other hand, for the continuous optimization problem, it is hard to determine the convexity of the objective function in (26). In the sequel, we will separately investigate the discrete part and the continuous part of Problem 3, and explore some properties of the ASE to simplify the optimization problem.

1) *Discrete Optimization:* The aim of the discrete optimization is to determine the optimal file set \mathcal{N}_c^* . To reduce the total number of choices that need to be considered, we observe the following property.

Property 1: In the interference-limited scenario, when the network is full-loaded, there exists an optimal \mathcal{N}_c^* in which the indexes of files are consecutive, i.e., $\mathcal{N}_c^* = \{n_1^b, n_1^b +$

$1, \dots, n_1^b + N_b^*\}$, with $N_b^* = |\mathcal{N}_b^*|$, and $n_1^b \in \{N_1 + 1, \dots, N - N_b^*\}$ being the index of the first file in \mathcal{N}_b^* .

Proof: Please refer to Appendix E. \blacksquare

Property 1 can significantly reduce the difficulty of solving the discrete optimization. By applying this property, noting that $\mathcal{N}_c = \mathcal{N}_2 \setminus \mathcal{N}_b$, the total number of choices that need to be considered for \mathcal{N}_c is cut down to $\sum_{N_b=1}^{N_2-C_2} \sum_{n_1^b=N_1+1}^{N-C_2-N_b+1} 1 = O(N_2^2)$. This allows us to use exhaustive search to solve the discrete optimization problem without losing optimality.

2) *Continuous Optimization:* The objective function of the continuous problem shown in (26) is complicated, whose convexity is hard to determine. However, $\text{ASE}_2(\mathcal{N}_c, \mathbf{T}, \mu)$ is a differentiable function w.r.t. \mathbf{T} , and the constraint set is convex. Therefore, we can use the gradient projection method (GPM) [34] to obtain a stationary point of the continuous problem. Even though GPM can solve the continuous problem properly, the convergence rate is highly dependent on the choice of the stepsize, which, however, may degrade the efficiency of the algorithm when selected improperly. Moreover, when calculating the derivative, an inverse of the Toeplitz matrix needs to be calculated, which will inevitably increase the computational complexity.

Therefore, to reduce the computation complexity in solving the continuous problem, we may consider using the following simple lower bound $\text{ASE}^l(\mathcal{N}_c, \mathbf{T}, \mu)$ as the objective function for Problem 1.

As shown in Appendix D, a lower bound on $\Psi_2(T_n, N_c, \mu)$ is given by

$$\Psi_2^l(T_n, N_c, \mu) = \sum_{\theta=0}^{M_2-U_2-1} \frac{p_{\Theta}(\theta)T_n}{\varrho_1 T_n + \varrho_2} + \frac{p_{\Theta}^s T_n}{\varrho_{1,1}(1)T_n + \varrho_{2,1}(1)}, \quad (27)$$

where $\beta = (D_2!)^{-\frac{1}{D_2}}$, $D_2 = M_2 - U_2 + 1 - \theta$, and ϱ_1 , ϱ_2 , $\varrho_{1,i}(x)$, and $\varrho_{2,i}(x)$ are given by

$$\varrho_1 = \begin{cases} \varrho_{1,1}(1) + \sum_{m=1}^{D_2-1} \frac{2(U_2)_m}{m!} \left(1 - \frac{m}{D_2}\right) & \mu < 1, \\ \times \left(\tilde{q}_m(\tau) - \tilde{F}_m(\tau)\right) \\ \varrho_{1,1}(1) + \varepsilon \sum_{m=1}^{D_2-1} \frac{2(U_2)_m}{m!} \left(1 - \frac{m}{D_2}\right) & \mu \geq 1, \\ \times \left(\tilde{B}_m(\tau) - \tilde{F}_m(\tau)\right) \end{cases} \quad (28)$$

$$\varrho_2 = \varrho_{2,1}(1) - \sum_{m=1}^{D_2-1} \frac{2(U_2)_m}{m!} \left(1 - \frac{m}{D_2}\right) \tilde{q}_m(\tau), \quad (29)$$

$$\varrho_{1,i}(x) = \begin{cases} 1 - \varrho_{2,i}(x) + F_2(ix\tau) & \mu < 1, \\ 1 - \varepsilon G(ix\tau) + \varepsilon F_2(ix\tau) & \mu \geq 1, \end{cases} \quad (30)$$

$$\varrho_{2,i}(x) = \varepsilon G(ix\tau) + (1 - \varepsilon)\mu^2 F_2\left(\frac{ix\tau}{\mu^{\alpha_2}}\right), \quad (31)$$

with $\tilde{B}_m(\tau) = \frac{1}{\alpha_2} \tau^{\frac{2}{\alpha_2}} B(m - \frac{2}{\alpha_2}, U_2 + \frac{2}{\alpha_2})$, and $\tilde{q}_m(\tau) = \varepsilon \tilde{B}_m(\tau) + (1 - \varepsilon)\mu^2 \tilde{F}_m(\frac{\tau}{\mu^{\alpha_2}})$.

By replacing the $\Psi_2(T_n, N_c, \mu)$ with $\Psi_2^l(T_n, N_c, \mu)$ in (14), a lower bound on the ASE, i.e., $\text{ASE}^l(\mathcal{N}_c, \mathbf{T}, \mu)$ can be obtained. Compared with the expression for $\text{ASE}(\mathcal{N}_c, \mathbf{T}, \mu)$ given in Section IV, when we calculate this bound, the calculation of the inverse of the Toeplitz matrix $\mathbf{W}_{D_2}(T_n, N_c, \mu)$ is avoided, thereby reducing the computational burden. Moreover, ϱ_1 , ϱ_2 , $\varrho_{1,i}(x)$, and $\varrho_{2,i}(x)$ are functions of variables (N_c, μ) , but are independent of T_n . This will ease the design of \mathbf{T} when \mathcal{N}_c is given.

Note that Property 1 still holds here, which can be proved by defining $f(x, y) \triangleq \min\{1, \frac{C_b}{N_2-y}\} \lambda_1 U_1 \Psi_1 - \lambda_2 U_2 \Psi_2^l(x, y, \mu)$ in Appendix E and following the similar procedure. Given \mathcal{N}_c and μ , the objective function in (26) will be replaced by its corresponding lower bound, denoted by $\text{ASE}_2^l(\mathcal{N}_c, \mathbf{T}, \mu)$. Therefore, the continuous optimization problem can be rewritten as follows.

Problem 4 (Lower Bound Optimization):

$$\begin{aligned} \max_{\mathbf{T}} \quad & \text{ASE}_2^l(\mathcal{N}_c, \mathbf{T}, \mu) \\ \text{s.t.} \quad & (23b). \end{aligned} \quad (32)$$

It can be easily observed that the optimization in Problem 4 is a convex problem. As shown in Appendix F, by using the KKT conditions, we can obtain the optimal solution to it as

$$T_n^\dagger = \begin{cases} 0, & a_n f(0) < \nu^\dagger, \\ 1, & a_n f(1) > \nu^\dagger, \\ x(T_n^\dagger, \nu^\dagger), & \text{otherwise,} \end{cases} \quad (33)$$

where

$$\begin{aligned} f(x) \triangleq & \frac{\partial \text{ASE}^l(\mathcal{N}_c, \mathbf{T}, \mu)}{a_n \partial T_n} \Big|_{T_n=x} = \lambda_2 U_2 \log_2(1 + \tau) \\ & \times \left[\sum_{\theta=0}^{M_2-U_2-1} \frac{p_{\Theta}(\theta) \varrho_2}{(\varrho_1 x + \varrho_2)^2} + \frac{p_{\Theta}^s \varrho_{2,1}(1)}{(\varrho_{1,1}(1)x + \varrho_{2,1}(1))^2} \right], \end{aligned} \quad (34)$$

where $x(T_n^\dagger, \nu^\dagger)$ denotes the root of equation $a_n f(x) = \nu^\dagger$, and the optimal Lagrangian multiplier ν^\dagger satisfies $\sum_{n \in \mathcal{N}_c} T_n^\dagger(\nu^\dagger) = C_2$. In addition, both $x(T_n^\dagger, \nu^\dagger)$ and ν^\dagger can be found by a simple bisection search.

B. IN Coefficient Optimization

In this part, we consider the following IN coefficient optimization problem given the solution of Problem 2 is obtained.

Problem 5 (IN Coefficient Optimization):

$$\begin{aligned} \text{ASE}^* = \max_{\mu} \quad & \text{ASE}^*(\mu) \\ \text{s.t.} \quad & (23c), \end{aligned} \quad (35)$$

where $\text{ASE}^*(\mu)$ is obtained by solving Problem 2.

Problem 5 is a one-dimensional optimization problem with only an orthant constraint [34]. We can effectively obtain its optimal solution using line search. Furthermore, in practice, the number of available antennas for IN at each SBS is limited. Therefore, the value of μ should be upper-bounded to prevent the value of Θ from being too large so that the IN scheme can perform effectively. To this end, we impose a constraint on μ to satisfy $\Theta \leq M_2 - U_2$. Note that a similar constraint

is considered in [35]. By substituting (12) into $\bar{\Theta} \leq M_2 - U_2$, we obtain the following constraint:

$$\begin{cases} 0 \leq \mu \leq \sqrt{\frac{\delta_A}{\delta_F}}, & \text{if } \delta_A \geq \delta_F, \\ 0 \leq \mu \leq \sqrt{\frac{\delta_A - 1}{\delta_F - 1}}, & \text{if } \delta_A < \delta_F, \end{cases} \quad (36)$$

where $\delta_A \triangleq M_2/U_2 \geq 1$ and $\delta_F \triangleq N_c/C_2 \geq 1$ represent the antenna gain and file diversity gain, respectively. It should be noted that (36) is not a necessary constraint for solving Problem 5. However, with this constraint, the process of solving Problem 5 will become more efficient.

Algorithm 1 Stationary Point for $\text{ASE}^l(\mathcal{N}_c, \mathbf{T}, \mu)$ Maximization

```

1: Initialize  $i = 0$ ,  $\mu^{(0)\dagger} \in [0, \sqrt{\delta_A}]$ , and  $\text{ASE}^\dagger = 0$ .
2: repeat
3:   Fix  $\mu^{(i)\dagger}$ .
4:   for  $N_c \in \{C_2, C_2 + 1, \dots, N_2\}$  do
5:     for all  $\mathcal{N}_c$  satisfying  $|\mathcal{N}_c| = N_c$  and Property 1 do
6:       Obtain  $T_n^\dagger$  for  $\forall n \in \mathcal{N}_c$  according to (33).
7:        $\mathbf{T}^\dagger(\mathcal{N}_c) \leftarrow [T_n^\dagger]_{n \in \mathcal{N}_c}$ , compute  $\text{ASE}' \triangleq \text{ASE}^l(\mathcal{N}_c, \mathbf{T}^\dagger(\mathcal{N}_c), \mu^{(i)\dagger})$ .
8:       if  $\text{ASE}^\dagger \leq \text{ASE}'$  then
9:         Set  $(\mathcal{N}_c^{(i+1)\dagger}, \mathbf{T}^{(i+1)\dagger}, \text{ASE}^\dagger) = (\mathcal{N}_c, \mathbf{T}^\dagger(\mathcal{N}_c), \text{ASE}')$ .
10:      end if
11:    end for
12:  end for
13:  Fix  $(\mathcal{N}_c^{(i+1)\dagger}, \mathbf{T}^{(i+1)\dagger})$ , obtain the optimal solution  $\mu^\dagger$  to Problem 5 with line search, and compute  $\text{ASE}' \triangleq \text{ASE}^l(\mathcal{N}_c^{(i+1)\dagger}, \mathbf{T}^{(i+1)\dagger}, \mu^\dagger)$ .
14:  if  $\text{ASE}^\dagger \leq \text{ASE}'$  then
15:    Set  $(\mu^{(i+1)\dagger}, \text{ASE}^\dagger) = (\mu^\dagger, \text{ASE}')$ .
16:  end if
17:   $i \leftarrow i + 1$ .
18: until Convergence.

```

C. Alternating Optimization

Algorithm 1 summarizes the whole procedure of alternately solving the cache placement optimization problem in Section V-A and the IN coefficient optimization problem in Section V-B. In each iteration, by using the KKT conditions, an optimal solution of Problem 4 can be obtained; by using exhaustive search, we can obtain an optimal solution for the discrete problem in (25). Therefore, when considering $\text{ASE}^l(\mathcal{N}_c, \mathbf{T}, \mu)$ as the objective function, we can obtain an optimal solution $(\mathcal{N}_c^\dagger, \mathbf{T}^\dagger)$ of Problem 2. In addition, given $(\mathcal{N}_c^\dagger, \mathbf{T}^\dagger)$, an optimal solution μ^\dagger for Problem 5 can be obtained using line search. The Step 8 ~ Step 10 and Step 14 ~ Step 16 in Algorithm 1 are used to ensure a solution not worse than the current one in each iteration when alternately solving Problem 2 and Problem 5. Therefore, when we set $\text{ASE}^l(\mathcal{N}_c, \mathbf{T}, \mu)$ as the objective function in Problem 1, the alternating procedure in Algorithm 1 converges to a stationary point of this problem [34, pp. 268]. We denote it

by $(\mathcal{N}_c^\dagger, \mathbf{T}^\dagger, \mu^\dagger)$. We take this stationary point as our *proposed policy* for maximizing $\text{ASE}(\mathcal{N}_c, \mathbf{T}, \mu)$ in Problem 1.

VI. PERFORMANCE EVALUATION

In this section, we evaluate the proposed joint hybrid caching policy and user-centric IN scheme in Matlab simulation.

A. Comparison Benchmarks

Note that Fig. 3(b) in Section IV provides a comparison of the system performance with (i.e., $\mu \neq 0$) and without IN (i.e., $\mu = 0$), indicates the advantages of our work with IN scheme over the works in [10]–[12], where interference management is not considered. In addition, [13] and [14] consider single-tier networks, which is different from our two-tier network layout. Hence, it is difficult to draw an equivalent performance comparison between our work and those two works due to the incompatibility of network settings. Therefore, we omit further performance comparison between our work and [10]–[14].

Instead, we compare the proposed method with two benchmarks that employ both caching and IN, MPC [15] and UDC [16]. For both benchmarks, each MBS selects the C_1 most popular files from the whole content library to store. The remaining files, forming the sub-set \mathcal{N}_2 , need to be further separated into two sets, whether to be served by SBSs or by MBSs via backhaul links. In MPC, each SBS selects the C_2 most popular files from \mathcal{N}_2 to store, and the remaining files in \mathcal{N}_2 are served by MBSs via backhaul links. In UDC, the C_b least popular files of \mathcal{N}_2 are served by MBSs via backhaul links, and each SBS randomly selects C_2 different files from the remaining $N_2 - C_b$ files to store, according to the uniform distribution. For each of the benchmarks, the IN scheme is adopted, where the optimal IN coefficient is obtained by solving Problem 5 with the corresponding given caching policy $(\mathcal{N}_c, \mathbf{T})$.

Moreover, for performance benchmarking, we further consider an upper bound of $\text{ASE}(\mathcal{N}_c, \mathbf{T}, \mu)$, denoted by $\text{ASE}^u(\mathcal{N}_c, \mathbf{T}, \mu)$, as shown in Appendix G. By replacing the objective function of Problem 1 with $\text{ASE}^u(\mathcal{N}_c, \mathbf{T}, \mu)$, we obtain an upper bound optimization problem, a stationary point of which, denoted by $(\mathcal{N}_c^\ddagger, \mathbf{T}^\ddagger, \mu^\ddagger)$, can be reached efficiently using the convex-concave procedure (CCP) approach [36], as illustrated in Appendix G. We repeat the procedure 5 times with different random initial values and choose the maximum $\text{ASE}^u(\mathcal{N}_c^\ddagger, \mathbf{T}^\ddagger, \mu^\ddagger)$ to obtain an approximate solution to the global optimum w.r.t. the upper bound. The result is shown with the legend ‘‘Upper Bound’’ in Figs. 4-7. Thus, even though we cannot obtain an optimal solution to Problem 1, we can evaluate how close the performance of our proposed policy is to the optimal one due to the relation $\text{ASE}(\mathcal{N}_c^\dagger, \mathbf{T}^\dagger, \mu^\dagger) \leq \text{ASE}^*(\mathcal{N}_c^*, \mathbf{T}^*, \mu^*) \leq \text{ASE}^u(\mathcal{N}_c^\ddagger, \mathbf{T}^\ddagger, \mu^\ddagger)$.

B. Simulation Results

Unless otherwise stated, the simulation settings are as follows: $M_1 = 32$, $M_2 = 16$, $U_1 = 32$, $U_2 = 4$, $P_1 = 46$ dBm, $P_2 = 23$ dBm, $\alpha_1 = \alpha_2 = 4$, $\lambda_1 = 1 \times 10^{-4} \text{ m}^{-2}$,

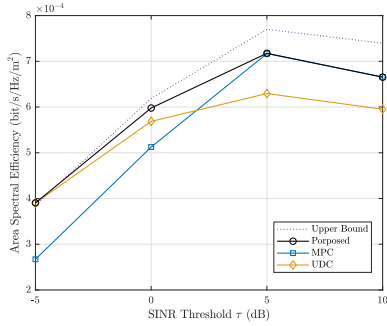


Fig. 4. ASE versus SINR threshold τ .

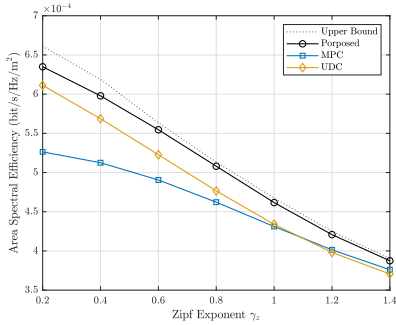


Fig. 5. ASE versus Zipf exponent γ_z .

$\lambda_2 = 5 \times 10^{-4} \text{ m}^{-2}$, $\lambda_u = 0.01 \text{ m}^{-2}$, $\tau = 0 \text{ dB}$, $N = 50$, $C_1 = 20$, $C_2 = 10$, $C_b = 3$, $\gamma_z = 0.4$. Figs. 4-7 plot the ASE versus the SINR threshold τ , the Zipf exponent γ_z , the backhaul capacity C_b , and the number of users served U_2 . From Figs. 4-7, we find that the maximum relative performance gap between our proposed policy (i.e., $\text{ASE}(\mathcal{N}_c^\dagger, \mathbf{T}^\dagger, \mu^\dagger)$) and the upper bound (i.e., $\text{ASE}^u(\mathcal{N}_c^\dagger, \mathbf{T}^\dagger, \mu^\dagger)$) is smaller than 8%, which indicates that the performance of our proposed policy is close to $\text{ASE}^*(\mathcal{N}_c^*, \mathbf{T}^*, \mu^*)$. Furthermore, the proposed caching policy outperforms MPC and UDC.

More specifically, from Fig. 4, we see that when τ is small (resp. large), the performance of the proposed method is almost the same as that of UDC (resp. MPC). This is because when τ is small, the SINR threshold is easy to reach, so file transmission can be successful even if the serving SBS of the typical user is not its nearest one, and hence caching more files in the network can increase the probability that the requested files are found in the SBSs. When τ is large, the typical user can only be served successfully by its nearest SBS, so ensuring the most popular files are successfully served is a better choice, which results in the least number of files cached in the SBSs.

From Fig. 5, we observe that the ASE of the network decreases with γ_z . This is different from the results in [7], [11], [19], where the network performance increases with γ_z . As a matter of fact, due to the dense deployment of the SBSs and the IN scheme adopted in our work, the ASE of the MBS tier is lower than that of the SBS tier. When γ_z increases, the requests of users are more concentrated on the most popular files, which, according to our hybrid caching policy, are mainly stored at MBSs. Hence, more users are served by the MBS

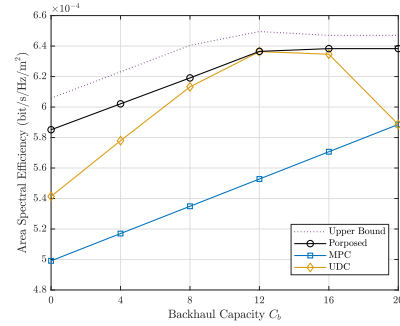


Fig. 6. ASE versus backhaul capacity C_b .

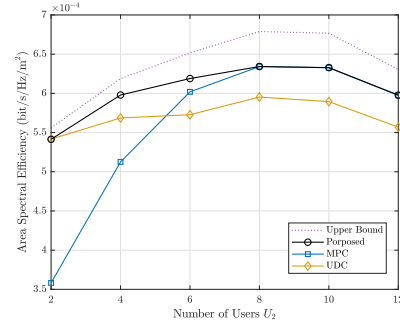


Fig. 7. ASE versus number of users served U_2 .

tier, leading to a decrease in ASE. Therefore, the proposed method gives higher ASE when the file popularity distribution is flatter.

Fig. 6 indicates that an increase of C_b generally leads to higher ASE for the proposed method and MPC, since the larger C_b is, the more files can be retrieved via backhaul links. When $C_b = 40$, the UDC policy lets each SBS choose $C_2 = 20$ files from \mathcal{N}_2 (of which the number of files is 20) to store, which is exactly the same as what the MPC policy does. However, the ASE of the proposed policy in this case is higher than that of UDC and MPC, since in the proposed policy, more files can be chosen to be served by SBSs rather than by backhaul links. In this case, the backhaul resource will not be fully utilized.

Fig. 7 depicts the relationship between the ASE and U_2 . We observe that when U_2 is small, the performance of UDC is close to that of the proposed method, whereas, with U_2 increasing, the performance of MPC gets closer to that of the proposed method. The reason for this is that when U_2 is small, almost all the IN requests received by SBSs can be satisfied, so caching more files in the SBSs leads to better performance. However, an increase of U_2 leads to an increase of IN missing probability ε , which degrades performance. To offset this negative effect, fewer files should be cached in the network, according to (12), which leads to $N_c = C_2$, corresponding to MPC.

VII. CONCLUSION

In this paper, we have considered random caching and IN design for cache-enabled multi-user multi-antenna HetNets. We derive the ASE over a two-tier network with hybrid file caching at both the MBSs and SBSs, where each SBS-user also

sends an IN request to the interfering SBSs within its IN range for interference suppression. We obtain a simple lower-bound expression for the ASE. Then, we optimize the caching policy and the IN coefficient toward ASE maximization. By partitioning the problem into two sub-problems and exploiting the properties of the ASE, an alternating optimization algorithm is proposed to obtain a stationary point. Our numerical results show that the proposed solution is close to the optimum, and it achieves significant performance gains over existing caching policies.

APPENDIX A DERIVATION OF $q_1(\mathcal{N}_c)$

To derive $q_1(\mathcal{N}_c)$, we need to calculate the complementary cumulative distribution function $\mathbb{P}[\Upsilon_{n,1} \geq \tau]$, where $\Upsilon_{n,1} = g_{01}Z_1^{-\alpha_1}/I_1$ is the received signal-to-interference ratio at u_0 , with Z_1 being the distance between u_0 and its serving MBS x_{10} and $I_1 = \sum_{x \in \Phi_1 \setminus x_{10}} g_{x_1} \|x\|^{-\alpha_1}$. The derivation for $\mathbb{P}[\Upsilon_{n,1} \geq \tau]$ has already been studied in [31], [33], we restate it here for completeness. Conditioning on $Z_1 = z_1$, we have

$$\mathbb{P}[\Upsilon_{n,1} \geq \tau] = \int_0^\infty \mathbb{P}[\Upsilon_{n,1} \geq \tau | Z_1 = z_1] f_{Z_1}(z_1) dz_1, \quad (37)$$

where $f_{Z_1}(z_1) = 2\pi\lambda_1 z_1 e^{-\pi\lambda_1 z_1^2}$ is the PDF of Z_1 . We have

$$\begin{aligned} \mathbb{P}[\Upsilon_{n,1} \geq \tau | Z_1 = z_1] &= \mathbb{E}_{I_1} [\mathbb{P}[g_{01} \geq \tau z_1^{\alpha_1} I_1]] \\ &\stackrel{(a)}{=} \mathbb{E}_{I_1} [\exp(-\tau z_1^{\alpha_1} I_1)] = \mathcal{L}_{I_1}(\tau z_1^{\alpha_1}), \end{aligned} \quad (38)$$

where (a) is due to $g_{01} \stackrel{d}{\sim} \Gamma(D_1, 1) = \Gamma(1, 1) = \text{Exp}(1)$; and $\mathcal{L}_{I_1}(\cdot)$ is the Laplace transform of I_1 , which is given by

$$\begin{aligned} \mathcal{L}_{I_1}(s) &= \mathbb{E}_{\Phi_1, g_{x_1}} \left[\exp \left(-s \sum_{x \in \Phi_1 \setminus x_{10}} g_{x_1} \|x\|^{-\alpha_1} \right) \right] \\ &\stackrel{(a)}{=} \mathbb{E}_{\Phi_1} \left[\prod_{x \in \Phi_1 \setminus x_{10}} \mathbb{E}_{g_{x_1}} [\exp(-s g_{x_1} \|x\|^{-\alpha_1})] \right] \\ &\stackrel{(b)}{=} \mathbb{E}_{\Phi_1} \left[\prod_{x \in \Phi_1 \setminus x_{10}} (1 + s \|x\|^{-\alpha_1})^{-U_1} \right] \\ &\stackrel{(c)}{=} \exp \left(-2\pi\lambda_1 \int_{z_1}^\infty (1 - (1 + sv^{-\alpha_1})^{-U_1}) v dv \right) \\ &= \exp(-\pi\lambda_1 z_1^2 F_1(s z_1^{-\alpha_1})), \end{aligned} \quad (39)$$

where $s = \tau z_1^{\alpha_1}$ and $F_1(x)$ is given by (10); (a) is due to the independence of different small-scale fading channels; (b) follows from $g_{x_1} \stackrel{d}{\sim} \Gamma(U_1, 1)$; (c) is from the probability generating functional for a PPP [33], and considering the conversion from Cartesian coordinate to polar coordinate. Substituting (38) and (39) into (37), and using $\int_0^\infty 2x e^{-Ax^2} dx = 1/A$, we can obtain Ψ_1 as (9).

APPENDIX B DERIVATION OF $\bar{\Theta}$

Denote by $\Phi'_{u,n}$ the users that request file n and are served by the SBS tier, the density of which is denoted by $\lambda'_{u,n}$. Since Φ_u^2 is a PPP and the file choices are independently made, $\Phi'_{u,n}$

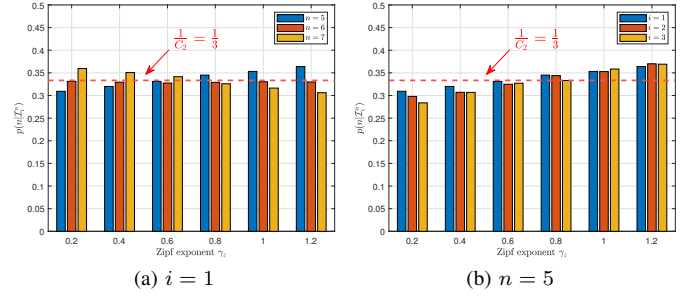


Fig. 8. Verification of the uniform distribution approximation for $p(n|\mathcal{I}_i^n)$. The simulation parameters are set to be the same as in Fig. 2. In this case, totally $I = \binom{4}{3} = 4$ file combinations are considered, i.e., $\mathcal{I}_1 = \{5, 6, 7\}$, $\mathcal{I}_2 = \{5, 6, 8\}$, $\mathcal{I}_3 = \{5, 7, 8\}$, $\mathcal{I}_4 = \{6, 7, 8\}$, whose corresponding caching probabilities are $p_1 = 0.4$, $p_2 = 0.3$, $p_3 = 0.2$, $p_4 = 0.1$, respectively. For the sub-figure (a), $\mathcal{I}_1^5 = \mathcal{I}_1^6 = \mathcal{I}_1^7 = \mathcal{I}_1$; for the sub-figure (b), $\mathcal{I}_1^5 = \mathcal{I}_1$, $\mathcal{I}_2^5 = \mathcal{I}_2$, and $\mathcal{I}_3^5 = \mathcal{I}_3$.

is a thinned PPP of Φ_u^2 . Let \mathcal{I}_i^n be the i -th combination from \mathcal{I}^n (recalling that \mathcal{I}^n is the set of combinations containing file n). Consider a typical SBS B_0 located at the origin and storing file n . The probability that it stores \mathcal{I}_i^n is $\frac{p_i}{T_n}$ (with $i \in \mathcal{I}^n$). Denote by $p(n|\mathcal{I}_i^n)$ the probability that a randomly chosen user associated with an SBS that stores \mathcal{I}_i^n requests file n . Since there are totally U_2 users associated with B_0 , the average number of connected users that request file n is $\bar{U}_{2,n} = \sum_{i \in \mathcal{I}^n} \frac{p_i}{T_n} U_2 p(n|\mathcal{I}_i^n)$.

Considering the density of SBSs that store file n is $\lambda_2 T_n$, we have $\lambda'_{u,n} = \lambda_2 T_n \bar{U}_{2,n} = \lambda_2 U_2 \sum_{i \in \mathcal{I}^n} p_i p(n|\mathcal{I}_i^n)$. We can see that $\lambda'_{u,n}$ highly depends on the combinations of files containing file n , i.e., \mathcal{I}^n , which has size $I^n = \binom{N_c-1}{C_2-1}$. When N_c and C_2 are large, it is unrealistic to calculate all the elements in \mathcal{I}^n . To this end, we use the uniform distribution to approximate $p(n|\mathcal{I}_i^n)$, i.e., $p(n|\mathcal{I}_i^n) \approx 1/C_2$. The accuracy of this approximation is verified by simulation in Fig. 8.² We can observe that the approximation is accurate with a moderate Zipf exponent. Then, $\lambda'_{u,n}$ can be approximated as

$$\lambda'_{u,n} \approx \frac{\lambda_2 U_2}{C_2} \sum_{i \in \mathcal{I}^n} p_i \stackrel{(a)}{=} \frac{\lambda_2 T_n U_2}{C_2}, \quad (40)$$

where (a) is due to (1).

Next, we will calculate the PMF of $\bar{\Theta}$. We first give the probability that a user sends a request to an SBS. Consider a user u_x located at x , who requests file $n \in \mathcal{N}_c$. This guarantees that u_x only can be served by SBSs. Consider an SBS B_0 located at the origin, which stores the file combination \mathcal{I}_i . Let Z_0 represent the distance between user u_x and its serving SBS.

Consider the case that $\mu < 1$. When $\|x\| \in [0, \mu Z_0]$, B_0 will receive an IN request from u_x if it is not the serving SBS of u_x , which means B_0 does not store file n , i.e., $n \notin \mathcal{I}_i$; otherwise, B_0 will be the serving SBS of u_x , which is contradictory.

²Given a file set \mathcal{N}_2 and its corresponding caching probability vector \mathbf{T} , we can obtain a set of caching probabilities, i.e., $p_i, \forall i \in \mathcal{I}$, corresponding to all the file combinations in \mathcal{I} , in the sense of least-squares, by solving the following optimization problem: $\min_{p_i, \forall i \in \mathcal{I}} \sum_{n \in \mathcal{N}_c} (\sum_{i \in \mathcal{I}^n} p_i - T_n)^2$, s.t. (1) and $0 \leq p_i \leq 1, \forall i \in \mathcal{I}$.

Therefore, the probability that u_x sends an IN request to B_0 , denoted by $p_s(x, n|\mathcal{I}_i)$, is given by

$$\begin{aligned} p_s(x, n|\mathcal{I}_i) &= \mathbb{1}\{n \notin \mathcal{I}_i\} \mathbb{P}[\|x\| \leq \mu Z_0] \\ &= \mathbb{1}\{n \notin \mathcal{I}_i\} \int_{\frac{\|x\|}{\mu}}^{\infty} f_{Z_0}(z) dz = \mathbb{1}\{n \notin \mathcal{I}_i\} e^{-\pi \lambda_2 T_n \frac{\|x\|^2}{\mu^2}}, \end{aligned} \quad (41)$$

where $f_{Z_0}(z) = 2\pi \lambda_2 T_n z e^{-\pi \lambda_2 T_n z^2}$ is the PDF of the distance between u_x and its serving SBS. Denote by $\Phi'_{u,n}$ the set of served users that request file n and send an IN request to SBS B_0 , which is a location-dependent thinned PPP of $\Phi'_{u,n}$ with density $\lambda'_{u,n}(x, n, i) = p_s(x, n|\mathcal{I}_i) \lambda'_{u,n}$. Denote by Θ_{in} the number of requests received at B_0 from the user in $\Phi'_{u,n}$, which equals the total number of users in $\Phi'_{u,n}$. Therefore, using the Campbell's Theorem, the mean of Θ_{in} is given by

$$\begin{aligned} \bar{\Theta}_{in} &= \int_{\mathbb{R}^2} \lambda'_{u,n}(x, n, i) dx \\ &\stackrel{(a)}{=} \frac{\lambda_2 T_n U_2}{C_2} \int_0^{2\pi} \int_0^{\infty} \mathbb{1}\{n \notin \mathcal{I}_i\} e^{-\pi \lambda_2 T_n \frac{r^2}{\mu^2}} r dr d\theta \\ &= \mathbb{1}\{n \notin \mathcal{I}_i\} \frac{U_2 \mu^2}{C_2}, \end{aligned} \quad (42)$$

where (a) is from the polar-Cartesian coordinate transformation, i.e., $dy = r dr d\theta$. We sum Θ_{in} , on the right-hand side of (42), for all the files in \mathcal{N}_c :

$$\bar{\Theta}_i = \sum_{n \in \mathcal{N}_c} \bar{\Theta}_{in} = \left(\sum_{n \in \mathcal{N}_c} 1 - \sum_{n \in \mathcal{I}_i} 1 \right) \frac{U_2 \mu^2}{C_2}. \quad (43)$$

Removing the condition that B_0 stores combination I_i , we have

$$\begin{aligned} \bar{\Theta} &= \sum_{i \in \mathcal{I}} p_i \bar{\Theta}_i = \sum_{i \in \mathcal{I}} p_i \left(\sum_{n \in \mathcal{N}_c} 1 - \sum_{n \in \mathcal{I}_i} 1 \right) \frac{U_2 \mu^2}{C_2} \\ &\stackrel{(a)}{=} \left(N_c - \sum_{i \in \mathcal{I}} \sum_{n \in \mathcal{I}_i} p_i \right) \frac{U_2 \mu^2}{C_2} \stackrel{(b)}{=} \left(N_c - \sum_{n \in \mathcal{N}_c} T_n \right) \frac{U_2 \mu^2}{C_2} \\ &= (N_c - C_2) \frac{U_2 \mu^2}{C_2}, \end{aligned} \quad (44)$$

where (a) is due to $N_c = \sum_{n \in \mathcal{N}_c} 1$, and (b) is from the relation $C_2 = \sum_{i \in \mathcal{I}} p_i C_2 = \sum_{i \in \mathcal{I}} \sum_{n \in \mathcal{I}_i} p_i \mathbb{1}\{n \in \mathcal{I}_i\} = \sum_{n \in \mathcal{N}_c} \sum_{i \in \mathcal{I}^n} p_i = \sum_{n \in \mathcal{N}_c} T_n$ [21].

When $\mu \geq 1$, we need to consider the following two cases: 1) when $\|x\| \in [0, Z_0]$, B_0 will receive an IN request from u_x if $n \notin \mathcal{I}_i$; 2) when $\|x\| \in (Z_0, \mu Z_0]$, B_0 will always receive a request from u_x . In this case, similar to (41), $p_s(x, n|\mathcal{I}_i)$ is given by

$$\begin{aligned} p_s(x, n|\mathcal{I}_i) &= \mathbb{1}\{n \notin \mathcal{I}_i\} \mathbb{P}[\|x\| \leq \mu Z_0] + \mathbb{P}[Z_0 < \|x\| \leq \mu Z_0] \\ &= (\mathbb{1}\{n \notin \mathcal{I}_i\} - 1) e^{-\pi \lambda_2 T_n \|x\|^2} + e^{-\pi \lambda_2 T_n \frac{\|x\|^2}{\mu^2}}. \end{aligned} \quad (45)$$

Similarly, $\bar{\Theta}_{in}$ can be obtained as

$$\bar{\Theta}_{in} = \int_{\mathbb{R}^2} p_s(x, n|\mathcal{I}_i) \lambda'_{u,n} dx = (\mathbb{1}\{n \notin \mathcal{I}_i\} - 1) \frac{U_2}{C_2} + \frac{U_2 \mu^2}{C_2}. \quad (46)$$

After summing $\bar{\Theta}_{in}$, on the right-hand side of (46), for all the files in \mathcal{N}_c , and removing the condition that B_0 stores combination I_i , we have

$$\bar{\Theta} = \sum_{i \in \mathcal{I}} p_i \sum_{n \in \mathcal{N}_c} \bar{\Theta}_{in} = \frac{N_c U_2 \mu^2}{C_2} - U_2. \quad (47)$$

Combining (44) and (47), we can obtain the expression for $\bar{\Theta}$ in (12).

APPENDIX C DERIVATION OF $q_2(\mathcal{N}_c, \mathbf{T}, \mu)$

A. Case $\mu < 1$

Based on the total probability formula, we have

$$\mathbb{P}[\Upsilon_{n,2} \geq \tau] = \sum_{\theta=0}^{\infty} p_{\Theta}(\theta) \Psi_{2,\Theta}(T_n, N_c, \mu, \theta), \quad (48)$$

where $\Psi_{2,\Theta}(T_n, N_c, \mu, \theta) \triangleq \mathbb{P}[\Upsilon_{n,2} \geq \tau | \Theta = \theta]$ is the STP conditioned on the number of received IN requests at the serving SBS of u_0 is $\Theta = \theta$. Conditioning on $Z_2 = z_2$, we have

$$\begin{aligned} \Psi_{2,\Theta}(T_n, N_c, \mu, \theta) &= \int_0^{\infty} \mathbb{P}[\Upsilon_{n,2} \geq \tau | Z_2 = z_2, \Theta = \theta] f_{Z_2}(z_2) dz_2 \\ &= \int_0^{\infty} \mathbb{P}[g_{02} \geq \tau z_2^{\alpha_2} I] f_{Z_2}(z_2) dz_2, \end{aligned} \quad (49)$$

where $I = \sum_{x \in \tilde{\Phi}_2} g_{x_2} \|x\|^{-\alpha_2}$, with $\tilde{\Phi}_2 = \Phi_2^a \cup \Phi_2^b \cup \Phi_2^c$; and $f_{Z_2}(z_2) = 2\pi \lambda_2 T_n z_2 \exp(-\pi \lambda_2 T_n z_2^2)$ is the PDF of the distance Z_2 . Note that applying the IN scheme will only change the density of the interfering SBSs of Type-A (for $\mu < 1$) or Type-B (for $\mu \geq 1$). Therefore, the densities of Φ_2^a , Φ_2^b , and Φ_2^c are $\lambda_2^a = \varepsilon \lambda_2 (1 - T_n)$, $\lambda_2^b = a b \lambda_2$, and $\lambda_2^c = \lambda_2$, with a and b given in (19). Since $g_{02} \stackrel{d}{\sim} \Gamma(D_2, 1)$ where $D_2 = \max\{M_2 - U_2 + 1 - \theta, 1\}$ (cf. Section III-D), using the CDF of g_{02} , we have [25]

$$\begin{aligned} \mathbb{P}[g_{02} \geq \tau z_2^{\alpha_2} I] &= \mathbb{E}_I \left[\sum_{m=0}^{D_2-1} \frac{s^m}{m!} I^m e^{-sI} \right] \\ &\stackrel{(a)}{=} \sum_{m=0}^{D_2-1} \frac{(-s)^m}{m!} \mathcal{L}_I^{(m)}(s), \end{aligned} \quad (50)$$

where $s = \tau z_2^{\alpha_2}$; $\mathcal{L}_I^{(m)}(s)$ denotes the m -th derivative of $\mathcal{L}_I(s)$; and (a) is due to the property of the Laplace transform, i.e., $\mathbb{E}_I [I^m e^{-sI}] = (-1)^m \mathcal{L}_I^{(m)}(s)$.

Furthermore, we have

$$\begin{aligned} \mathcal{L}_I(s) &= \mathbb{E}_I [\exp(-sI)] \\ &= \mathbb{E}_I \left[\exp \left(-s \sum_{x \in \tilde{\Phi}_2} g_{x_2} \|x\|^{-\alpha_2} \right) \right] \\ &= \mathbb{E}_{\tilde{\Phi}_2} \left[\prod_{x \in \tilde{\Phi}_2} \mathbb{E}_{g_{x_2}} [\exp(-s g_{x_2} \|x\|^{-\alpha_2})] \right] \\ &\stackrel{(a)}{=} \mathbb{E}_{\tilde{\Phi}_2} \left[\prod_{x \in \tilde{\Phi}_2} (1 + s \|x\|^{-\alpha_2})^{-U_2} \right] \end{aligned}$$

$$\stackrel{(b)}{=} \underbrace{\exp\left(-2\pi \sum_{i=a}^c \lambda_2^i \int_{\Omega_i} (1 - (1 + sv^{-\alpha_2})^{-U_2}) v dv\right)}_{\triangleq \chi(s)}, \quad (51)$$

where (a) is due to $g_{x_2} \stackrel{d}{\sim} \Gamma(U_2, 1)$, (b) is from the probability generating functional for a PPP and the polar-Cartesian coordinate transformation, and the intervals $\Omega_a = [0, \mu z_2]$, $\Omega_b = [\mu z_2, z_2]$, and $\Omega_c = [z_2, +\infty)$ are given in Section III-C. Denote the exponent in (51) by $\chi(s)$ as shown above. We have

$$\begin{aligned} \chi(s) &= -2\pi(\lambda_2^a \mathcal{H}_0^{\mu z_2} - \lambda_2^b \mathcal{H}_{\mu z_2}^{\mu z_2} - \lambda_2^c \mathcal{H}_{z_2}^\infty) \\ &= -2\pi(\lambda_2^a (\mathcal{H}_0^\infty - \mathcal{H}_{\mu z_2}^\infty) - \lambda_2^b (\mathcal{H}_{\mu z_2}^\infty - \mathcal{H}_{z_2}^\infty) - \lambda_2^c \mathcal{H}_{z_2}^\infty) \\ &= -\pi\lambda_2^a (G(s) - (\mu z_2)^2 F_2(s(\mu z_2)^{-\alpha_2})) \\ &\quad - \pi\lambda_2^b ((\mu z_2)^2 F_2(s(\mu z_2)^{-\alpha_2}) - z_2^2 F_2(s z_2^{-\alpha_2})) \\ &\quad - \pi\lambda_2^c z_2^2 F_2(s z_2^{-\alpha_2}), \end{aligned} \quad (52)$$

where $\mathcal{H}_x^y = \int_x^y h(v)dv$, with $h(v) \triangleq (1 - (1 + sv^{-\alpha_2})^{-U_2})v$; and $G(x)$ is given by (20). In (52), \mathcal{H}_x^∞ can be obtained from (39) when $x > 0$, whereas \mathcal{H}_0^∞ can be obtained by $\lim_{z \rightarrow 0} z^2 F_2(s z^{-\alpha_2}) = G(s)$. Considering $\mathcal{L}'_I(s) = \mathcal{L}_I(s)\chi'(s)$ and the Leibniz formula, we have

$$\mathcal{L}_I^{(m)}(s) = \sum_{k=0}^{m-1} \binom{m-1}{k} \chi^{(m-k)}(s) \mathcal{L}_I^{(k)}(s), \quad (53)$$

where $\chi^{(k)}(s)$ denotes the k -th derivative of $\chi(s)$, and is given by

$$\begin{aligned} \chi^{(k)}(s) &= 2\pi \sum_{i=a}^c \lambda_2^i \int_{\Omega_i} (-1)^k (U_2)_k \frac{(v^{-\alpha_2})^k v}{(1 + sv^{-\alpha_2})^{U_2+k}} dv \\ &= (-1)^k (U_2)_k 2\pi \left\{ \lambda_2^a \left[\frac{1}{\alpha_2} s^{\frac{2}{\alpha_2}-k} B\left(k - \frac{2}{\alpha_2}, U_2 + \frac{2}{\alpha_2}\right) \right. \right. \\ &\quad \left. \left. - (\mu z_2)^2 \tilde{F}_k(s(\mu z_2)^{-\alpha_2}) \right] + \lambda_2^b \left[(\mu z_2)^2 \tilde{F}_k(s(\mu z_2)^{-\alpha_2}) \right. \right. \\ &\quad \left. \left. - z_2^2 \tilde{F}_k(s z_2^{-\alpha_2}) \right] + \lambda_2^c z_2^2 \tilde{F}_k(s z_2^{-\alpha_2}) \right\}, \end{aligned} \quad (54)$$

where $(U)_n = U(U+1)\cdots(U+n-1)$ is the Pochhammer symbol, $B(x, y)$ is the Beta function, and $\tilde{F}_k(x)$ is given in (21). The second equality above is due to [37, (3.194)]. Let

$$w_0 = -\frac{\chi(s)}{\pi z_2^2 \lambda_2}, \quad w_m = \frac{(-s)^m}{\pi z_2^2 \lambda_2 m!} \chi^{(m)}(s), \quad (55)$$

we thus have $\mathcal{L}_I(s)|_{s=\tau z_2^{\alpha_2}} = \exp(-\pi z_2^2 w_0)$. Substituting $s = \tau z_2^{\alpha_2}$ into (52) and (54), after some manipulation, the expressions of w_0 and w_m are obtained as (17) and (18).

Let $x_m = \frac{1}{m!} (-s)^m \mathcal{L}_I^{(m)}(s)$. From (53), we have

$$x_m = \sum_{k=0}^{m-1} \frac{m-k}{m} \left(\frac{(-s)^{m-k}}{(m-k)!} \chi^{(m-k)}(s) \right) x_k. \quad (56)$$

Considering the recurrence relation in (56), we have

$$x_m = \pi z_2^2 \sum_{k=0}^{m-1} \frac{m-k}{m} w_{m-k} x_k, \quad x_0 = \exp(-\pi z_2^2 w_0). \quad (57)$$

Next, we will obtain an explicit expression for x_m by solving the recurrent relation in (57). We first define two power series $\tilde{W}(z)$ and $X(z)$ as

$$\tilde{W}(z) \triangleq \sum_{m=0}^{\infty} w_m z^m, \quad X(z) \triangleq \sum_{m=0}^{\infty} x_m z^m. \quad (58)$$

The derivative of $\tilde{W}(z)$ is $\tilde{W}^{(1)}(z) = \sum_{m=0}^{\infty} m w_m z^{m-1}$, the derivative of $X(z)$ is $X^{(1)}(z) = \sum_{m=0}^{\infty} m x_m z^{m-1}$, and the product of $\tilde{W}(z)$ and $X(z)$ is $\tilde{W}(z)X(z) = \sum_{m=0}^{\infty} (\sum_{i=0}^m w_{m-i} x_i) z^m$. Then, from (57), we have

$$zX^{(1)}(z) = \pi z_2^2 z \tilde{W}^{(1)}(z) X(z). \quad (59)$$

By solving the above differential equation, we have $X(z) = C \exp(\pi z_2^2 \tilde{W}(z))$, where C is a constant to be determined. Since $X(0) = x_0 = \mathcal{L}_I(s)$ and $\tilde{W}(0) = w_0$, from (57), we can obtain $C = \exp(-2\pi z_2^2 w_0)$, and

$$X(z) = \exp\left(\pi z_2^2 (\tilde{W}(z) - 2w_0)\right). \quad (60)$$

Recalling from (49), we have

$$\begin{aligned} &\Psi_{2,\Theta}(T_n, N_c, \mu, \theta) \\ &= \mathbb{E}_{Z_2} [\mathbb{P}[g_{02} \geq \tau z_2^{\alpha_2} I]] = \mathbb{E}_{Z_2} \left[\sum_{m=0}^{D_2-1} x_m \right] \\ &= \mathbb{E}_{Z_2} \left[\sum_{m=0}^{D_2-1} \frac{1}{m!} \frac{d^m}{dz^m} X(z) \Big|_{z=0} \right] \\ &= \sum_{m=0}^{D_2-1} \frac{1}{m!} \frac{d^m}{dz^m} \mathbb{E}_{Z_2} [X(z)] \Big|_{z=0} \\ &= \sum_{m=0}^{D_2-1} \frac{1}{m!} \frac{d^m}{dz^m} \int_0^\infty \exp(\pi z_2^2 (\tilde{W}(z) - 2w_0)) f_{Z_2}(z_2) dz_2 \Big|_{z=0} \\ &= T_n \sum_{m=0}^{D_2-1} \frac{1}{m!} \frac{d^m}{dz^m} (T_n + 2w_0 - \tilde{W}(z))^{-1} \Big|_{z=0} \\ &\stackrel{(a)}{=} T_n \left\| \left[(T_n + 2w_0) \mathbf{I}_{D_2} - \tilde{\mathbf{W}}_{D_2}(T_n, N_c, \mu) \right]^{-1} \right\|_1, \end{aligned} \quad (61)$$

where $D_2 = \max\{M_2 - U_2 + 1 - \theta, 1\}$, and $\mathbf{W}_{D_2}(T_n, N_c, \mu) \triangleq (T_n + 2w_0) \mathbf{I}_{D_2} - \tilde{\mathbf{W}}_{D_2}(T_n, N_c, \mu)$ is given in (16). Let $Q(z) \triangleq T_n (T_n + 2w_0 - \tilde{W}(z))^{-1}$, from [38, p. 14], (a) is due to that the first D_2 coefficients of $Q(z)$ is the first column of the matrix $T_n \mathbf{W}_{D_2}(T_n, N_c, \mu)^{-1}$, and their sum equals the L_1 induced norm of this matrix. Further considering (48), we can obtain $\Psi_2(T_n, N_c, \mu)$ as in (15), where the second term is due to the fact $\sum_{\theta=M_2-U_2}^\infty p_\Theta(\theta) = \frac{\gamma(M_2-U_2, \bar{\Theta})}{\Gamma(M_2-U_2)}$ for the Poisson random variable $\bar{\Theta}$.

B. Case $\mu \geq 1$

When $\mu \geq 1$, the integration intervals in (51), (52), and (54) become $\Omega_a = [0, z_2]$, $\Omega_b = [z_2, \mu z_2]$, and $\Omega_c = [\mu z_2, +\infty)$. Then, following the same procedure as the case $\mu < 1$, we can

complete the proof of the case $\mu \geq 1$. We omit the detailed steps due to the page limitation.

APPENDIX D

DERIVATION OF THE LOWER BOUND ON $\Psi_2(T_n, N_c, \mu)$

We define $\mathbf{p} \triangleq [1, 1, \dots, 1]_{D_2 \times 1}^T$ and $\mathbf{q} \triangleq \mathbf{W}_{D_2}(T_n, N_c, \mu)\mathbf{p}$, with $\mathbf{W}_{D_2}(T_n, N_c, \mu)$ given in (16). Then, we have $\mathbf{p} = \mathbf{W}_{D_2}(T_n, N_c, \mu)^{-1}\mathbf{q}$. Considering the inequality $\|\mathbf{p}\|_1 \leq \|\mathbf{W}_{D_2}(T_n, N_c, \mu)^{-1}\|_1 \|\mathbf{q}\|_1$, we have

$$\|\mathbf{W}_{D_2}(T_n, N_c, \mu)^{-1}\|_1 \geq \frac{\|\mathbf{p}\|_1}{\|\mathbf{q}\|_1}. \quad (62)$$

Since $\|\mathbf{p}\|_1 = D_2$ and $\|\mathbf{q}\|_1 = T_n + w_0 + \sum_{m=1}^{D_2-1} [T_n + w_0 - (D_2 - m)w_m]$, we can obtain the following lower bound on $\|\mathbf{W}_{D_2}(T_n, N_c, \mu)^{-1}\|_1$:

$$\|\mathbf{W}_{D_2}(T_n, N_c, \mu)^{-1}\|_1 \geq \frac{1}{T_n + w_0 - \sum_{m=1}^{D_2-1} \left(1 - \frac{m}{D_2}\right) w_m}. \quad (63)$$

Replacing $\|\mathbf{W}_{D_2}(T_n, N_c, \mu)^{-1}\|_1$ in (15) with the right-hand side term in (63), and after some manipulation, we can obtain the lower bound $\Psi_2^l(T_n, N_c, \mu)$ shown in (27).

APPENDIX E

PROOF OF PROPERTY 1

Let $(\mathcal{N}_c^*, \mathbf{T}^*)$ and $\mathcal{N}_b^* = \mathcal{N}_c \setminus \mathcal{N}_c^*$ denote an optimal solution to Problem 2. Suppose \mathcal{N}_b^* has S elements and is represented by $\mathcal{N}_b^* = \{n_1^*, n_2^*, \dots, n_S^*\}$, the elements of which are non-consecutive and sorted in ascending order. Note that the non-consecutiveness of the elements in \mathcal{N}_b^* is equivalent to $n_S^* - n_1^* + 1 > S$, which is also equivalent to the existence of an index j , $1 \leq j < S$, such that $n_j^* + 1 < n_{j+1}^*$. We now construct from $(\mathcal{N}_c^*, \mathbf{T}^*)$ another optimal solution, where the indexes of files in \mathcal{N}_b^* are consecutive.

Denote by $f(x, y) \triangleq \min\{1, \frac{C_b}{N_2 - y}\} \lambda_1 U_1 \Psi_1 - \lambda_2 U_2 \Psi_2(x, y, \mu)$. We first show that $f(T_{n_j^*+1}, N_c^*) = 0$.

Suppose $f(T_{n_j^*+1}, N_c^*) < 0$. Consider the alternative solution $\mathcal{N}_b^{\text{up}} = \{n_2^*, \dots, n_j^*, n_j^* + 1, n_{j+1}^*, \dots, n_S^*\}$, $T_{n_1^*}^{\text{up}} = T_{n_j^*+1}^*$, and $T_n^{\text{up}} = T_n^*$ for $\forall n \in \mathcal{N}_c^* \setminus \{n_j^* + 1\}$. Then, we have $\text{ASE}(\mathcal{N}_c^{\text{up}}, \mathbf{T}^{\text{up}}, \mu) - \text{ASE}(\mathcal{N}_c^*, \mathbf{T}^*, \mu) = \log_2(1 + \tau)(a_{n_j^*+1} - a_{n_1^*})f(T_{n_j^*+1}, N_c^*)$. Since $n_1^* < n_{n_j^*+1}^*$, we have $a_{n_1^*} > a_{n_j^*+1}$, and thus $\text{ASE}(\mathcal{N}_c^{\text{up}}, \mathbf{T}^{\text{up}}, \mu) - \text{ASE}(\mathcal{N}_c^*, \mathbf{T}^*, \mu) > 0$, which contradicts with the optimality of $(\mathcal{N}_c^*, \mathbf{T}^*)$.

Suppose $f(T_{n_j^*+1}, N_c^*) > 0$. Consider the alternative solution $\mathcal{N}_b^{\text{dn}} = \{n_1^*, \dots, n_j^*, n_j^* + 1, n_{j+1}^*, \dots, n_{S-1}^*\}$, $T_{n_S^*}^{\text{dn}} = T_{n_j^*+1}^*$, and $T_n^{\text{dn}} = T_n^*$ for $\forall n \in \mathcal{N}_c^* \setminus \{n_j^* + 1\}$. Then, we have $\text{ASE}(\mathcal{N}_c^{\text{dn}}, \mathbf{T}^{\text{dn}}, \mu) - \text{ASE}(\mathcal{N}_c^*, \mathbf{T}^*, \mu) = \log_2(1 + \tau)(a_{n_j^*+1} - a_{n_S^*})f(T_{n_j^*+1}, N_c^*)$. Similarly to the previous case, we can show that this is strictly greater than zero, leading to contradiction.

Now, since $f(T_{n_j^*+1}, N_c^*) = 0$, we can construct a new solution $\mathcal{N}' = \{n'_1, n'_2, \dots, n'_S\}$ as equal to either $\mathcal{N}_b^{\text{up}}$ or $\mathcal{N}_b^{\text{dn}}$, and we have $\text{ASE}(\mathcal{N}', \mathbf{T}', \mu) - \text{ASE}(\mathcal{N}_c^*, \mathbf{T}^*, \mu) = 0$, which means $(\mathcal{N}', \mathbf{T}')$ is also optimal. Note that in either case, we have $n'_S - n'_1 + 1 < n_S^* - n_1^* + 1$.

Relabel the elements in \mathcal{N}'_b as $\{n'_1, \dots, n'_S\}$, and relabel \mathcal{N}'_b as \mathcal{N}_b^* . Note that by doing so, we have decreased the value of $n'_S - n'_1 + 1$ without losing optimality. If the elements of \mathcal{N}_b^* are still non-consecutive, we can repeat the above procedure to decrease the value of $n'_S - n'_1 + 1$ each time, until it reaches $n'_S - n'_1 + 1 = S$. At this point, the elements of \mathcal{N}_b^* are consecutive (and \mathcal{N}_b^* is still optimal).

APPENDIX F

SOLUTION TO PROBLEM 4

The Lagrange function of Problem 4 is given by

$$\begin{aligned} \mathcal{L} = & -\text{ASE}^l(\mathcal{N}_c, \mathbf{T}, \mu) - \sum_{n \in \mathcal{N}_c} \lambda_n T_n \\ & + \sum_{n \in \mathcal{N}_c} \vartheta_n (T_n - 1) + \nu \left(\sum_{n \in \mathcal{N}_c} T_n - C_2 \right), \end{aligned} \quad (64)$$

where $\boldsymbol{\lambda} \triangleq [\lambda_n]_{n \in \mathcal{N}_c}$ and $\boldsymbol{\vartheta} \triangleq [\vartheta_n]_{n \in \mathcal{N}_c}$ are the Lagrange multipliers associated with the constraint $0 \leq T_n \leq 1$, $\forall n \in \mathcal{N}_c$; and ν is the Lagrange multiplier associated with the constraint $\sum_{n \in \mathcal{N}_c} T_n = C_2$. Then, the derivative of \mathcal{L} w.r.t. T_n is

$$\frac{\partial \mathcal{L}}{\partial T_n} = -a_n f(T_n) - \lambda_n + \vartheta_n + \nu, \quad (65)$$

where $f(x)$ is given in (34).

The KKT conditions can be written as

$$0 \leq T_n^\dagger \leq 1, \quad \sum_{n \in \mathcal{N}_c} T_n^\dagger = C_2, \quad (66a)$$

$$\lambda_n^\dagger \geq 0, \quad \vartheta_n^\dagger \geq 0, \quad (66b)$$

$$\lambda_n^\dagger T_n^\dagger = 0, \quad \vartheta_n^\dagger (T_n^\dagger - 1) = 0, \quad (66c)$$

$$\left. \frac{\partial \mathcal{L}}{\partial T_n} \right|_{T_n = T_n^\dagger} = 0, \quad (66d)$$

where λ_n^\dagger and ϑ_n^\dagger , for $\forall n \in \mathcal{N}_c$, are the optimal value of λ_n and ϑ_n , respectively. From (66d), we have $\vartheta_n^\dagger = a_n f(T_n^\dagger) + \lambda_n^\dagger - \nu^\dagger$. Since $f(x)$ is a decreasing function of x , we have the following three cases: If $\nu^\dagger > a_n f_{\max}(x) = a_n f(0)$, considering the dual feasibility in (66b), the complementary slackness condition in (66c) can only hold if $\lambda_n^\dagger > 0$ and $\vartheta_n^\dagger = 0$, implying that $T_n^\dagger = 0$. If $\nu^\dagger < a_n f_{\min}(x) = a_n f(1)$, the conditions in (66b) and (66c) yield $\lambda_n^\dagger = 0$ and $T_n^\dagger = 1$. If $a_n f(1) \leq \nu^\dagger \leq a_n f(0)$, (66b) and (66c) can only hold if $\lambda_n^\dagger = \vartheta_n^\dagger = 0$, so from (65) and (66d), we have $\nu_n^\dagger = a_n f(T_n^\dagger)$. By solving the equation $\nu_n^\dagger = a_n f(T_n^\dagger)$ as well as (66a), we can obtain T_n^\dagger and its corresponding ν_n^\dagger .

APPENDIX G

CCP APPROACH FOR MAXIMIZING $\text{ASE}^u(\mathcal{N}_c, \mathbf{T}, \mu)$ FOR THE PROBLEM IN (26)

A. An Upper Bound on $\text{ASE}(\mathcal{N}_c, \mathbf{T}, \mu)$

From Appendix C, we have

$$\begin{aligned} \Psi_{2,\Theta} &= \mathbb{E}_{I,Z_2} [\mathbb{P}[g_{02} \geq \tau z_2^{\alpha_2} I]] \\ &\stackrel{(a)}{\leq} 1 - \mathbb{E}_{I,Z_2} \left[(1 - \exp(-\beta \tau z_2^{\alpha_2} I))^{D_2} \right] \end{aligned}$$

$$\begin{aligned}
 &= 1 - \mathbb{E}_{I, Z_2} \left[\sum_{i=0}^{D_2} (-1)^i \binom{D_2}{i} \exp(-i\beta\tau z_2^{\alpha_2} I) \right] \\
 &= \sum_{i=1}^{D_2} (-1)^{i+1} \binom{D_2}{i} \mathbb{E}_{I, Z_2} [\exp(-i\beta\tau z_2^{\alpha_2} I)] \\
 &= \sum_{i=1}^{D_2} (-1)^{i+1} \binom{D_2}{i} \mathbb{E}_{Z_2} [\mathcal{L}_I(i\beta\tau z_2^{\alpha_2})] \triangleq \Psi_{2,\Theta}^u, \quad (67)
 \end{aligned}$$

where (a) is due to $g_{02} \stackrel{d}{\sim} \Gamma(D_2, 1)$ and a lower bound on the incomplete gamma function $\frac{\gamma(D, x)}{\Gamma(D)}$, i.e., $(1 - e^{-\beta x})^D \leq \frac{\gamma(D, x)}{\Gamma(D)}$ [39]. Since $\mathcal{L}_I(\tau z_2^{\alpha_2}) = \exp(-\pi z_2^2 w_0)$, we can obtain $\mathcal{L}_I(i\beta\tau z_2^{\alpha_2})$ by replacing τ with $i\beta\tau$, i.e., $\mathcal{L}_I(i\beta\tau z_2^{\alpha_2}) = \exp(-\pi z_2^2 A_i)$, with $A_i \triangleq \varepsilon(1 - T_n)G(i\beta\tau) + a(1 - \varepsilon)\mu^2 F_2\left(\frac{i\beta\tau}{\mu^{\alpha_2}}\right) + bT_n F_2(i\beta\tau)$, $\beta = (D_2!)^{-1/D_2}$. We then have $\mathbb{E}_{Z_2}[\mathcal{L}_I(i\beta\tau z_2^{\alpha_2})] = \int_0^\infty \exp(-\pi z_2^2 A_i) f_{Z_2}(z_2) dz_2 = \frac{T_n}{\varrho_{1,i}(\beta)T_n + \varrho_{2,i}(\beta)}$, with $\varrho_{1,i}(x)$ and $\varrho_{2,i}(x)$ defined in (30) and (31). Note that $\Psi_2^u(T_n, N_c, \mu) = \sum_{\theta=0}^\infty p_\Theta(\theta) \Psi_{2,\Theta}^u$. After some manipulation, we obtain an upper bound on $\Psi_2(T_n, N_c, \mu)$ given by

$$\begin{aligned}
 &\Psi_2^u(T_n, N_c, \mu) \\
 &= \sum_{\theta=0}^{M_2-U_2-1} p_\Theta(\theta) \sum_{i=1}^{D_2} (-1)^{i+1} \binom{D_2}{i} \frac{T_n}{\varrho_{1,i}(\beta)T_n + \varrho_{2,i}(\beta)} \\
 &\quad + \frac{p_\Theta^s T_n}{\varrho_{1,1}(1)T_n + \varrho_{2,1}(1)}, \quad (68)
 \end{aligned}$$

where $\varrho_{1,i}(x)$ and $\varrho_{2,i}(x)$ are given in (30) and (31). By replacing the $\Psi_2(T_n, N_c, \mu)$ with $\Psi_2^u(T_n, N_c, \mu)$ in (14), we can obtain an upper bound on the ASE, denoted by $\text{ASE}^u(\mathcal{N}_c, \mathbf{T}, \mu)$.

B. CCP Approach for Maximizing $\text{ASE}^u(\mathcal{N}_c, \mathbf{T}, \mu)$

When setting $\text{ASE}^u(\mathcal{N}_c, \mathbf{T}, \mu)$ as the objective function of Problem 1, the objective function in (26) will be replaced by its corresponding upper bound, denoted by $\text{ASE}_2^u(\mathcal{N}_c, \mathbf{T}, \mu)$. It is easy to see that we can decompose $\text{ASE}_2^u(\mathcal{N}_c, \mathbf{T}, \mu)$ as

$$\text{ASE}_2^u(\mathcal{N}_c, \mathbf{T}, \mu) = \eta_1(\mathcal{N}_c, \mathbf{T}, \mu) - \eta_2(\mathcal{N}_c, \mathbf{T}, \mu), \quad (69)$$

with

$$\begin{aligned}
 \eta_1(\mathcal{N}_c, \mathbf{T}, \mu) &\triangleq \lambda_2 U_2 \log_2(1 + \tau) \sum_{n \in \mathcal{N}_c} a_n \left[\frac{p_\Theta^s T_n}{\varrho_{1,1}(1)T_n + \varrho_{2,1}(1)} \right. \\
 &\quad \left. + \sum_{\theta=0}^{M_2-U_2-1} p_\Theta(\theta) \sum_{i \in \mathcal{D}_o} \binom{D_2}{i} \frac{T_n}{\varrho_{1,i}(\beta)T_n + \varrho_{2,i}(\beta)} \right], \\
 \eta_2(\mathcal{N}_c, \mathbf{T}, \mu) &\triangleq \lambda_2 U_2 \log_2(1 + \tau) \sum_{n \in \mathcal{N}_c} a_n \sum_{\theta=0}^{M_2-U_2-1} p_\Theta(\theta) \\
 &\quad \times \sum_{i \in \mathcal{D}_e} \binom{D_2}{i} \frac{T_n}{\varrho_{1,i}(\beta)T_n + \varrho_{2,i}(\beta)}, \quad (70)
 \end{aligned}$$

where \mathcal{D}_o and \mathcal{D}_e denote the sets of all the odd numbers and even numbers in the set $\{1, 2, \dots, D_2\}$. Therefore, the continuous optimization problem can be reformulated as follows.

Problem 6 (Upper Bound Optimization):

$$\max_{\mathbf{T}} \eta_1(\mathcal{N}_c, \mathbf{T}, \mu) - \eta_2(\mathcal{N}_c, \mathbf{T}, \mu)$$

$$\text{s.t.} \quad (23\text{b}). \quad (71)$$

Note that $\eta_1(\mathcal{N}_c, \mathbf{T}, \mu)$ and $\eta_2(\mathcal{N}_c, \mathbf{T}, \mu)$ are differentiable and concave w.r.t. \mathbf{T} . Therefore, Problem 6 is a DC programming problem, a stationary point of which can be found by using the CCP approach [36]. Under CCP, $-\eta_2(\mathcal{N}_c, \mathbf{T}, \mu)$ is linearized using first-order Taylor expansion around the point obtained in the previous iteration, so that the objective function becomes concave and the linearized problem is convex. CCP proceeds by solving such a sequence of convex problems.

Specifically, at the j -th iteration, we consider the following problem:

$$\begin{aligned}
 \mathbf{T}^{(j)\dagger} &= \arg \max_{\mathbf{T}} \eta_1(\mathcal{N}_c, \mathbf{T}, \mu) - \tilde{\eta}_2(\mathcal{N}_c, \mathbf{T}, \mu | \mathbf{T}^{(j-1)\dagger}) \\
 &\text{s.t.} \quad (23\text{b}), \quad (72)
 \end{aligned}$$

where $\mathbf{T}^{(j)\dagger}$ denotes the optimal value of \mathbf{T} at the j -th iteration; and $\tilde{\eta}_2(\mathcal{N}_c, \mathbf{T}, \mu | \mathbf{T}^{(j-1)\dagger}) \triangleq \eta_2(\mathcal{N}_c, \mathbf{T}^{(j-1)\dagger}, \mu) + (\mathbf{T} - \mathbf{T}^{(j-1)\dagger})^T \nabla \eta_2(\mathcal{N}_c, \mathbf{T}^{(j-1)\dagger}, \mu)$, with $\nabla \eta_2(\mathcal{N}_c, \mathbf{T}, \mu)$ being the gradient of $\eta_2(\mathcal{N}_c, \mathbf{T}, \mu)$ w.r.t. \mathbf{T} .

It can be easily observed that the optimization in (72) is a convex problem. Similar to the procedures shown in Appendix F, by using the KKT conditions, we can obtain the optimal solution to the problem in (72) as

$$T_n^{(j)\dagger} = \begin{cases} 0, & a_n \tilde{f}(0) < \nu^\dagger, \\ 1, & a_n \tilde{f}(1) > \nu^\dagger, \\ x(T_n^{(j-1)\dagger}, \nu^\dagger), & \text{otherwise,} \end{cases} \quad (73)$$

where $\tilde{f}(x) \triangleq \eta_1'(\mathcal{N}_c, x, \mu) - \eta_2'(\mathcal{N}_c, T_n^{(j-1)\dagger}, \mu)$, with

$$\begin{aligned}
 \eta_1'(\mathcal{N}_c, x, \mu) &\triangleq \left. \frac{\partial \eta_1(\mathcal{N}_c, \mathbf{T}, \mu)}{a_n \partial T_n} \right|_{T_n=x} = \lambda_2 U_2 \log_2(1 + \tau) \\
 &\quad \times \left[\frac{p_\Theta^s \varrho_{2,1}(1)}{(\varrho_{1,1}(1)x + \varrho_{2,1}(1))^2} + \sum_{\theta=0}^{M_2-U_2-1} p_\Theta(\theta) \right. \\
 &\quad \left. \times \sum_{i \in \mathcal{D}_o} \binom{D_2}{i} \frac{\varrho_{2,i}(\beta)}{(\varrho_{1,i}(\beta)x + \varrho_{2,i}(\beta))^2} \right], \\
 \eta_2'(\mathcal{N}_c, x, \mu) &\triangleq \left. \frac{\partial \eta_2(\mathcal{N}_c, \mathbf{T}, \mu)}{a_n \partial T_n} \right|_{T_n=x} = \lambda_2 U_2 \log_2(1 + \tau) \\
 &\quad \times \sum_{\theta=0}^{M_2-U_2-1} p_\Theta(\theta) \sum_{i \in \mathcal{D}_e} \binom{D_2}{i} \frac{\varrho_{2,i}(\beta)}{(\varrho_{1,i}(\beta)x + \varrho_{2,i}(\beta))^2}, \quad (74)
 \end{aligned}$$

where $x(T_n^{(j-1)\dagger}, \nu^\dagger)$ denotes the root of equation $a_n \tilde{f}(x) = \nu^\dagger$, and the optimal Lagrangian multiplier ν^\dagger satisfies $\sum_{n \in \mathcal{N}_c} T_n^{(j)\dagger}(\nu) = C_2$.

Thus, following the framework of CCP, by iteratively solving the optimization problem in (72) according to (73), a stationary point of Problem 6 can be obtained. By following the similar procedures introduced in Section V-C, we can finally reach a stationary point for Problem 1, when taking the upper bound as the objective function.

REFERENCES

- [1] N. Bhushan, J. Li, D. Malladi, R. Gilmore, D. Brenner, A. Damjanovic, R. Sukhvasi, C. Patel, and S. Geirhofer, "Network densification: the dominant theme for wireless evolution into 5G," *IEEE Commun. Mag.*, vol. 52, no. 2, pp. 82–89, Feb. 2014.

- [2] J. G. Andrews, S. Buzzi, W. Choi, S. V. Hanly, A. Lozano, A. C. K. Soong, and J. C. Zhang, "What will 5G be?" *IEEE J. Sel. Areas Commun.*, vol. 32, no. 6, pp. 1065–1082, Jun. 2014.
- [3] X. Ge, H. Cheng, M. Guizani, and T. Han, "5G wireless backhaul networks: Challenges and research advances," *IEEE Netw.*, vol. 28, no. 6, pp. 6–11, Nov. 2014.
- [4] D. Lopez-Perez, I. Guvenc, G. de la Roche, M. Kountouris, T. Quek, and J. Zhang, "Enhanced intercell interference coordination challenges in heterogeneous networks," *IEEE Wirel. Commun.*, vol. 18, no. 3, pp. 22–30, Jun. 2011.
- [5] D. Liu, B. Chen, C. Yang, and A. F. Molisch, "Caching at the wireless edge: Design aspects, challenges, and future directions," *IEEE Commun. Mag.*, vol. 54, no. 9, pp. 22–28, Sep. 2016.
- [6] E. Bastug, M. Bennis, and M. Debbah, "Living on the edge: The role of proactive caching in 5G wireless networks," *IEEE Commun. Mag.*, vol. 52, no. 8, pp. 82–89, Aug. 2014.
- [7] Y. Cui and D. Jiang, "Analysis and optimization of caching and multicasting in large-scale cache-enabled heterogeneous wireless networks," *IEEE Trans. Wireless Commun.*, vol. 16, no. 1, pp. 250–264, Jan. 2017.
- [8] E. G. Larsson, O. Edfors, F. Tufvesson, and T. L. Marzetta, "Massive MIMO for next generation wireless systems," *IEEE Commun. Mag.*, vol. 52, no. 2, pp. 186–195, Feb. 2014.
- [9] L. Liu, R. Chen, S. Geirhofer, K. Sayana, Z. Shi, and Y. Zhou, "Downlink MIMO in LTE-advanced: SU-MIMO vs. MU-MIMO," *IEEE Commun. Mag.*, vol. 50, no. 2, pp. 140–147, Feb. 2012.
- [10] D. Liu and C. Yang, "Caching policy toward maximal success probability and area spectral efficiency of cache-enabled HetNets," *IEEE Trans. Commun.*, vol. 65, no. 6, pp. 2699–2714, Jun. 2017.
- [11] S. Kuang, X. Liu, and N. Liu, "Analysis and optimization of random caching in SKS-tier multi-antenna multi-user HetNets," *IEEE Trans. Commun.*, vol. 67, no. 8, pp. 5721–5735, Aug. 2019.
- [12] S. Kuang and N. Liu, "Analysis and optimization of random caching in multi-antenna small-cell networks with limited backhaul," *IEEE Trans. Veh. Technol.*, vol. 68, no. 8, pp. 7789–7803, Aug. 2019.
- [13] D. Jiang and Y. Cui, "Enhancing performance of random caching in large-scale wireless networks with multiple receive antennas," *IEEE Trans. Wireless Commun.*, vol. 18, no. 4, pp. 2051–2065, Apr. 2019.
- [14] X. Xu and M. Tao, "Modeling, analysis, and optimization of caching in multi-antenna small-cell networks," *IEEE Trans. Wireless Commun.*, vol. 18, no. 11, pp. 5454–5469, Nov. 2019.
- [15] E. Baştuğ, M. Bennis, M. Kountouris, and M. Debbah, "Cache-enabled small cell networks: modeling and tradeoffs," *EURASIP J. Wirel. Commun. Netw.*, vol. 2015, no. 1, pp. 1–11, Dec. 2015.
- [16] S. Tamoor-ul Hassan, M. Bennis, P. H. J. Nardelli, and M. Latva-Aho, "Modeling and analysis of content caching in wireless small cell networks," in *ISWCS*, Aug. 2015, pp. 765–769.
- [17] B. N. Bharath, K. G. Nagananda, and H. V. Poor, "A learning-based approach to caching in heterogeneous small cell networks," *IEEE Trans. Commun.*, vol. 64, no. 4, pp. 1674–1686, Apr. 2016.
- [18] J. Wen, K. Huang, S. Yang, and V. O. K. Li, "Cache-enabled heterogeneous cellular networks: Optimal tier-level content placement," *IEEE Trans. Wireless Commun.*, vol. 16, no. 9, pp. 5939–5952, Sep. 2017.
- [19] S. Zhang and J. Liu, "Optimal probabilistic caching in heterogeneous IoT networks," *IEEE Internet Things J.*, vol. 7, no. 4, pp. 3404–3414, Apr. 2020.
- [20] J. Yang, C. Ma, B. Jiang, G. Ding, G. Zheng, and H. Wang, "Joint optimization in cached-enabled heterogeneous network for efficient industrial IoT," *IEEE J. Sel. Areas Commun.*, vol. 38, no. 5, pp. 831–844, May 2020.
- [21] Y. Cui, D. Jiang, and Y. Wu, "Analysis and optimization of caching and multicasting in large-scale cache-enabled wireless networks," *IEEE Trans. Wireless Commun.*, vol. 15, no. 7, pp. 5101–5112, Jul. 2016.
- [22] L. Yang, F. Zheng, W. Wen, and S. Jin, "Analysis and optimization of random caching in mmwave heterogeneous networks," *IEEE Trans. Veh. Technol.*, vol. 69, no. 9, pp. 10 140–10 154, Sep. 2020.
- [23] R. M. Amer, H. ElSawy, J. Kibilda, M. Butt, and N. Marchetti, "Performance analysis and optimization of cache-assisted CoMP for clustered D2D networks," *IEEE Trans. Mob. Comput.*, vol. 1233, to be published, 2020.
- [24] S. Akoum and R. W. Heath, "Interference coordination: Random clustering and adaptive limited feedback," *IEEE Trans. Signal Process.*, vol. 61, no. 7, pp. 1822–1834, Apr. 2013.
- [25] C. Li, J. Zhang, M. Haenggi, and K. B. Letaief, "User-centric intercell interference nulling for downlink small cell networks," *IEEE Trans. Commun.*, vol. 63, no. 4, pp. 1419–1431, Apr. 2015.
- [26] Y. Cui, Y. Wu, D. Jiang, and B. Clerckx, "User-centric interference nulling in downlink multi-antenna heterogeneous networks," *IEEE Trans. Wireless Commun.*, vol. 15, no. 11, pp. 7484–7500, Nov. 2016.
- [27] C. Zhu and W. Yu, "Stochastic modeling and analysis of user-centric network MIMO systems," *IEEE Trans. Commun.*, vol. 66, no. 12, pp. 6176–6189, Dec. 2018.
- [28] C. Li, J. Zhang, J. G. Andrews, and K. B. Letaief, "Success probability and area spectral efficiency in multiuser MIMO HetNets," *IEEE Trans. Commun.*, vol. 64, no. 4, pp. 1544–1556, Apr. 2016.
- [29] G. Hattab and D. Cabric, "Coverage and rate maximization via user association in multi-antenna HetNets," *IEEE Trans. Wireless Commun.*, vol. 17, no. 11, pp. 7441–7455, Nov. 2018.
- [30] A. K. Gupta, H. S. Dhillon, S. Vishwanath, and J. G. Andrews, "Downlink multi-antenna heterogeneous cellular network with load balancing," *IEEE Trans. Commun.*, vol. 62, no. 11, pp. 4052–4067, Nov. 2014.
- [31] J. G. Andrews, F. Baccelli, and R. K. Ganti, "A tractable approach to coverage and rate in cellular networks," *IEEE Trans. Commun.*, vol. 59, no. 11, pp. 3122–3134, Nov. 2011.
- [32] T. Bai and R. W. Heath Jr, "Asymptotic coverage probability and rate in massive MIMO networks," *arXiv preprint arXiv:1305.2233*, 2013.
- [33] M. Haenggi, *Stochastic Geometry for Wireless Networks*. Cambridge, U.K.: Cambridge Univ. Press, 2012.
- [34] Dimitri P. Bertsekas, *Nonlinear Programming 2nd*. Belmont, MA, USA: Athena Scientific, 1999.
- [35] K. Hosseini, C. Zhu, A. A. Khan, R. S. Adve, and W. Yu, "Optimizing the MIMO cellular downlink: Multiplexing, diversity, or interference nulling?" *IEEE Trans. Commun.*, vol. 66, no. 12, pp. 6068–6080, Dec. 2018.
- [36] T. Lipp and S. Boyd, "Variations and extension of the convex–concave procedure," *Optim. Eng.*, vol. 17, no. 2, pp. 263–287, Jun. 2016.
- [37] I. S. Gradshteyn and I. M. Ryzhik, *Table of Integrals, Series, and Products*. New York, USA: Elsevier, 2014.
- [38] P. Henrici, *Applied and Computational Complex Analysis, Volume 1: Power Series, Integration, Conformal Mapping, Location of Zeros*. New York, USA: John Wiley & Sons, 1988.
- [39] H. Alzer, "On some inequalities for the incomplete gamma function," *Math. Comput.*, vol. 66, no. 218, pp. 771–779, Apr. 1997.